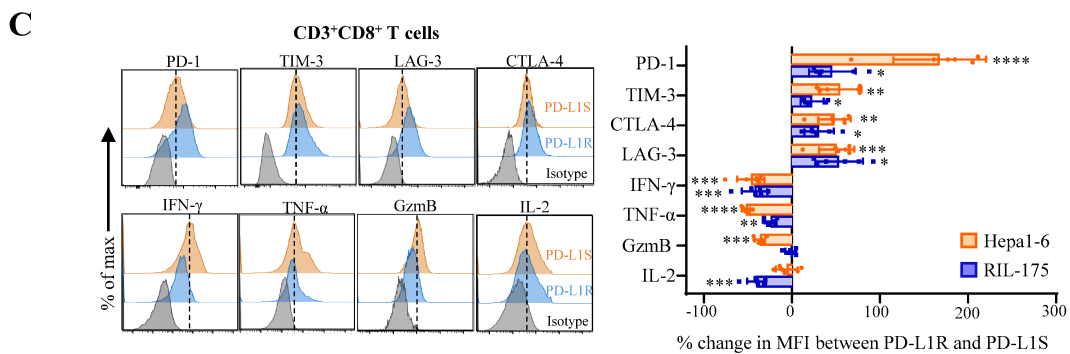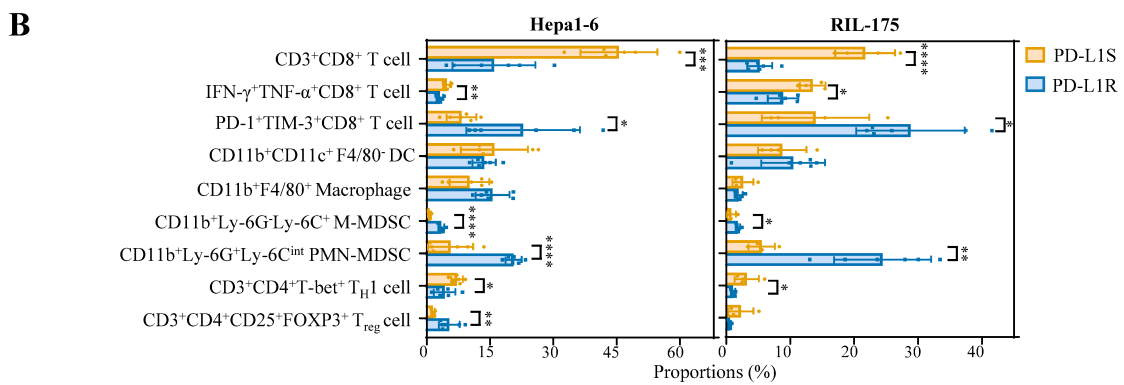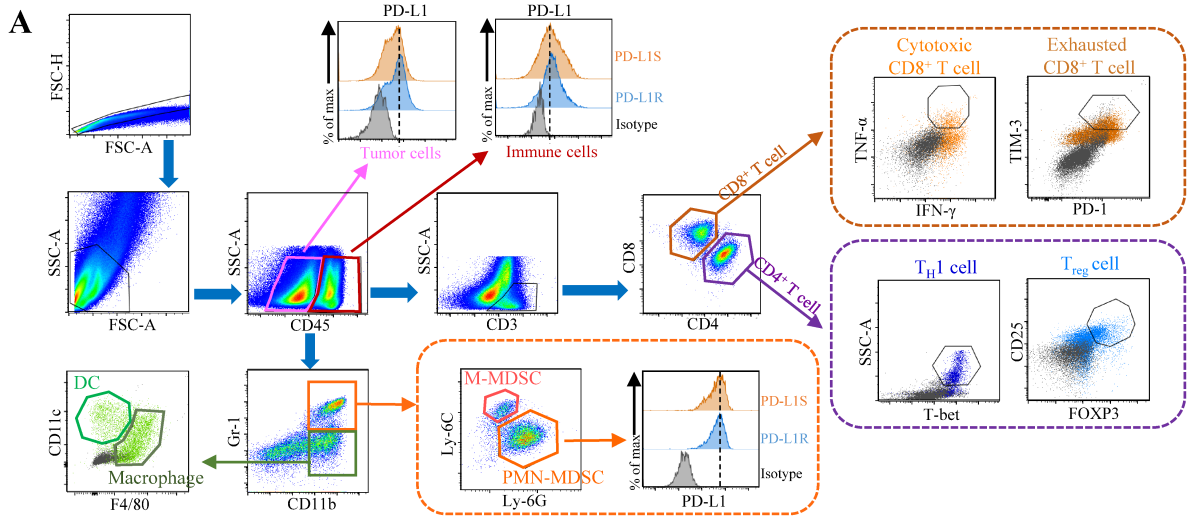**Supplementary Figures**

Supplementary Figure 1. Growth of anti-PD-L1-sensitive and -resistant tumors in immunodeficient mice.

BALB/c nude mice were intrahepatically inoculated by Hepa1-6 (5×10^6) or RIL-175 (5×10^5) PD-L1S and PD-L1R cells. At day 18, the tumors were excised and weighed. **(A)** Representative liver tumor photos and tumor weights of indicated groups in Hepa1-6 and **(B)** RIL-175 models at the endpoint (n = 6 to 8). Data represent as mean ± SD. Statistical significance was determined by unpaired two-tailed Student's t-test.

Supplemental material

BMJ Publishing Group Limited (BMJ) disclaims all liability and responsibility arising from any reliance placed on this supplemental material which has been supplied by the author(s)

Gut

Supplementary Figure 2. Gating strategy for immune profiling in this study.

(A) Gating strategy of indicated immune cells in lymphoid and myeloid lineages by multi-color flow cytometry. Dark grey dot plot refers to isotype control. Dash line indicates the peak of the PD-L1S sample. **(B)** Proportions of $CD3^+CD8^+$ T cells, $CD11b^+CD11c^+F4/80^-$ DCs, $CD11b^+F4/80^+$ macrophages, $CD11b^+Ly\text{-}6G^-Ly\text{-}6C^+$ M-MDSCs, $CD11b^+Ly\text{-}6G^+Ly\text{-}6C^{int}$ PMN-MDSCs, $CD3^+CD4^+T\text{-}bet^+ T_H1$ cells and $CD3^+CD4^+CD25^+FOXP3^+ T_{reg}$ cells in $CD45^+$ leukocytes, as well as $IFN\text{-}\gamma^+TNF\text{-}\alpha^+$ cells and $PD\text{-}1^+TIM\text{-}3^+$ cells among $CD8^+$ T cells from anti-PD-L1-treated tumors (n = 4 to 6 per group). **(C)** Representative overlay histogram and percentage changes of immune checkpoints (PD-1, TIM-3, CTLA-4 and LAG-3) and effector cytokines (IFN-γ, TNF-α, GzmB and IL-2) in $CD8^+$ T cells between PD-L1R and PD-L1S tumors with anti-PD-L1 treatment (n = 6). Dash line indicates the peak of the PD-L1S sample. Data represent as mean ± SD. Statistical significance was determined by unpaired two-tailed Student's t-test. *$P < 0.05$; **$P < 0.01$; ***$P < 0.001$; ****$P < 0.0001$.

Supplemental material

BMJ Publishing Group Limited (BMJ) disclaims all liability and responsibility arising from any reliance placed on this supplemental material which has been supplied by the author(s)

Gut

A

B
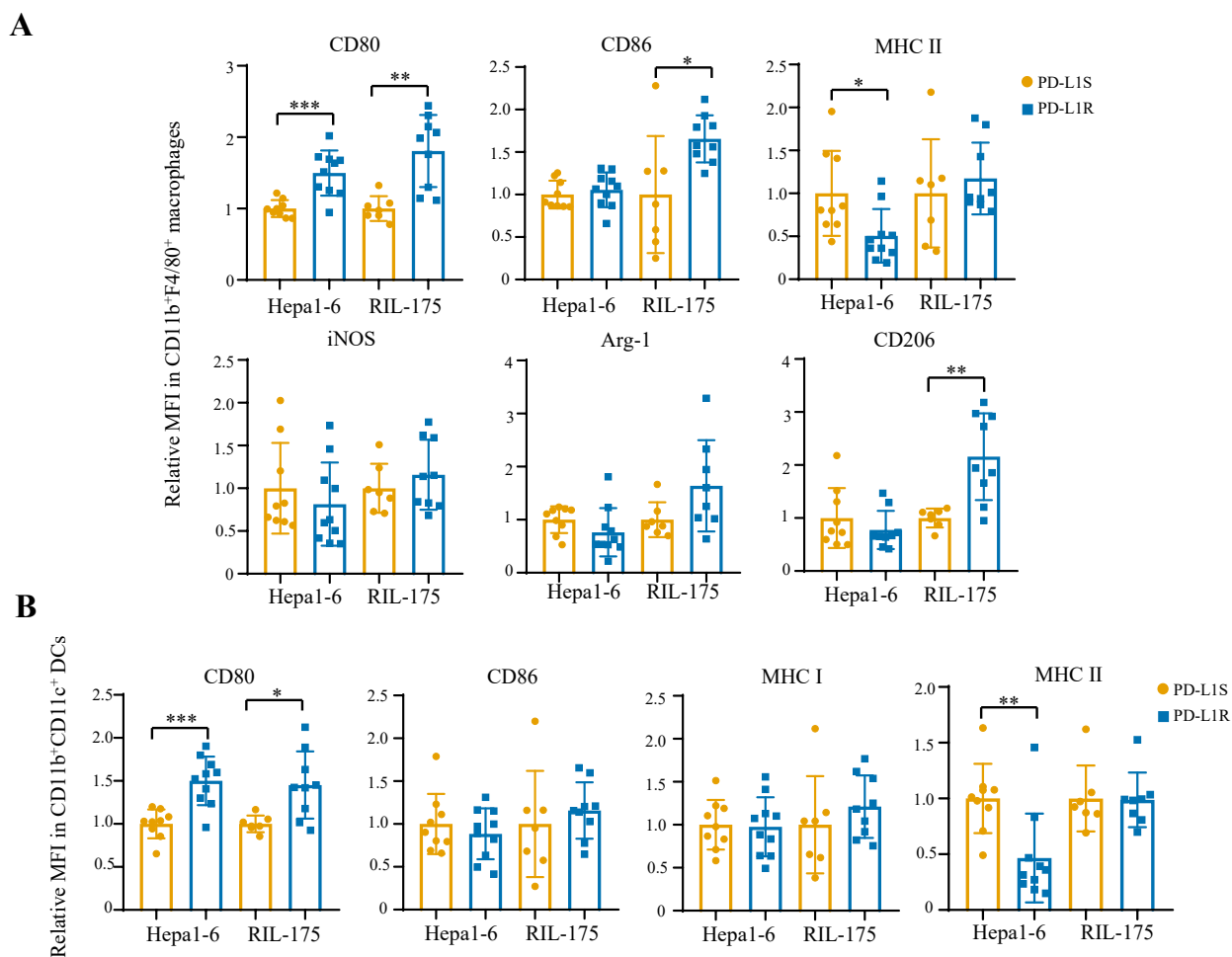
Supplementary Figure 3. Phenotypic characterization of macrophages and DCs in anti-PD-L1-sensitive and -resistant models.

Relative mean fluorescence intensity (MFI) of co-stimulatory molecules CD80 and CD86, antigen presentation molecules MHC class I and II, and immunosuppressive molecules iNOS, Arg-1 and CD206 in **(A)** CD11b$^+$F4/80$^+$ macrophages and **(B)** CD11b$^+$CD11c$^+$ DCs from Hepa1-6 and RIL-175 sensitive and resistant tumors (n = 7 to 10). The relative MFI are normalized to the molecule expressions in the PD-L1S group. Data represent as mean ± SD. Statistical significance was determined by unpaired two-tailed Student's t-test. *$P < 0.05$; **$P < 0.01$; ***$P < 0.001$.
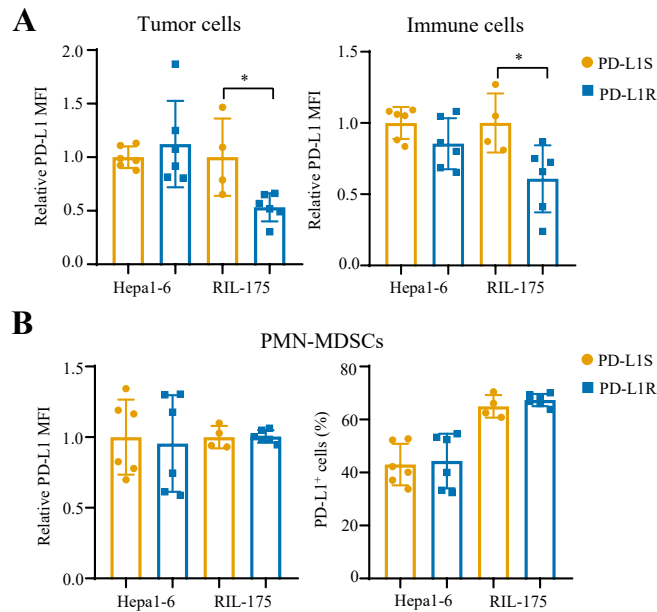
Supplementary Figure 4. PD-L1 expression in tumor cells and immune cells in anti-PD-L1-sensitive and -resistant models.

(A) Relative PD-L1 expression levels indicated by MFI in CD45^{-} tumor cells, CD45^{+} immune cells and (B) PMN-MDSCs, as well as PD-L1^{+} cell proportions in PMN-MDSCs from PD-L1S and PD-L1R tumors. Data of PD-L1 MFI are normalized to PD-L1S expression level. Data represent as mean ± SD. Statistical significance was determined by unpaired two-tailed Student's t-test. *$P < 0.05$.
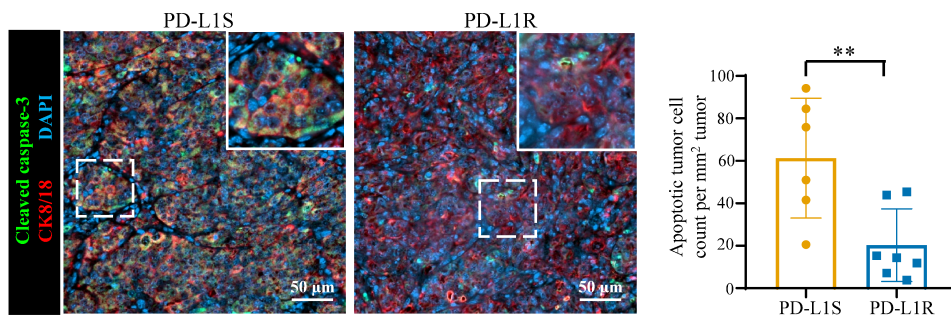
Supplementary Figure 5. Co-immunofluorescence staining of apoptotic tumor cells in anti-PD-L1-sensitive and resistant tumor tissues.

Representative co-immunofluorescence images of tumor cell marker cytokeratin 8/18 (CK8/18; red) and apoptotic cell marker cleaved caspase-3 (green) in Hepa1-6 PD-L1S and PD-L1R tumors. DAPI (blue) indicates the nuclei staining. Scale bars, 50 μm. The dot plot (right) shows the quantification of apoptotic tumor cells per mm^2 tumor area (n = 6 to 7). Data represent as mean ± SD. Statistical significance was determined by unpaired two-tailed Student's t-test. *$P < 0.01$.
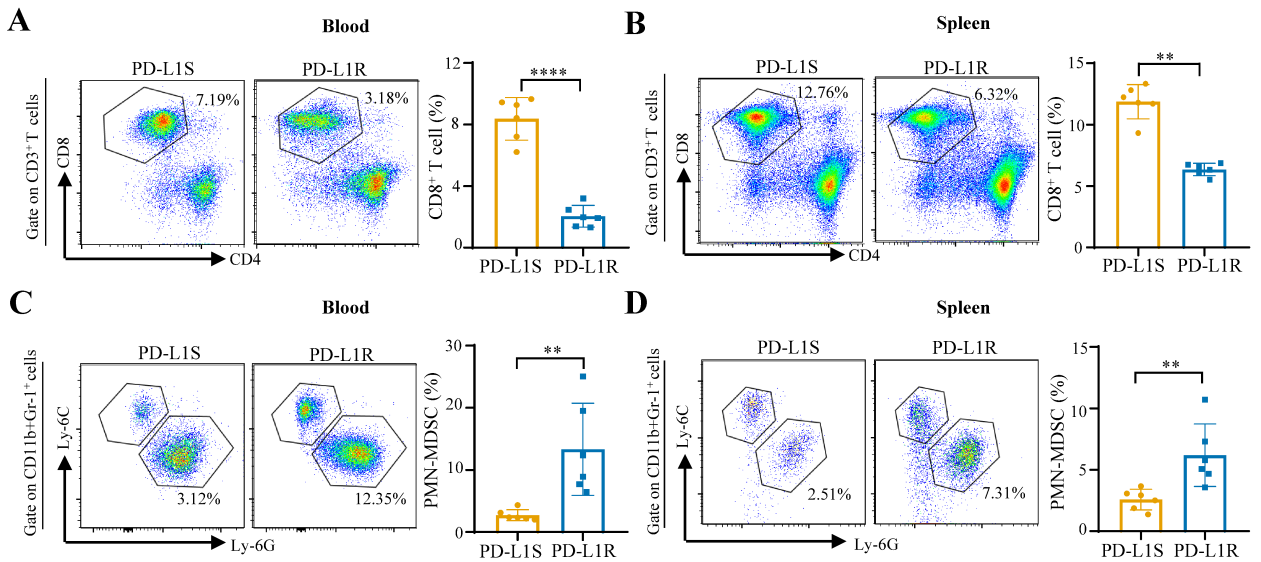
Supplementary Figure 6. Proportions of CD8+ T cells and PMN-MDSCs in blood and spleen of tumor-bearing mice.

(A) Representative flow cytometry dot plots and proportions of CD8+ T cells in blood and **(B)** spleen of bearing Hepa1-6 PD-L1S or PD-L1R tumors under anti-PD-L1 treatment (n = 6). **(C)** Representative flow cytometry dot plots and proportions of PMN-MDSCs in blood and **(D)** spleen of mice bearing Hepa1-6 PD-L1S or PD-L1R tumors under anti-PD-L1 treatment (n = 6). Data represent as mean ± SD. Statistical significance was determined by unpaired two-tailed Student's t-test. **$P < 0.01$; ****$P < 0.0001$.
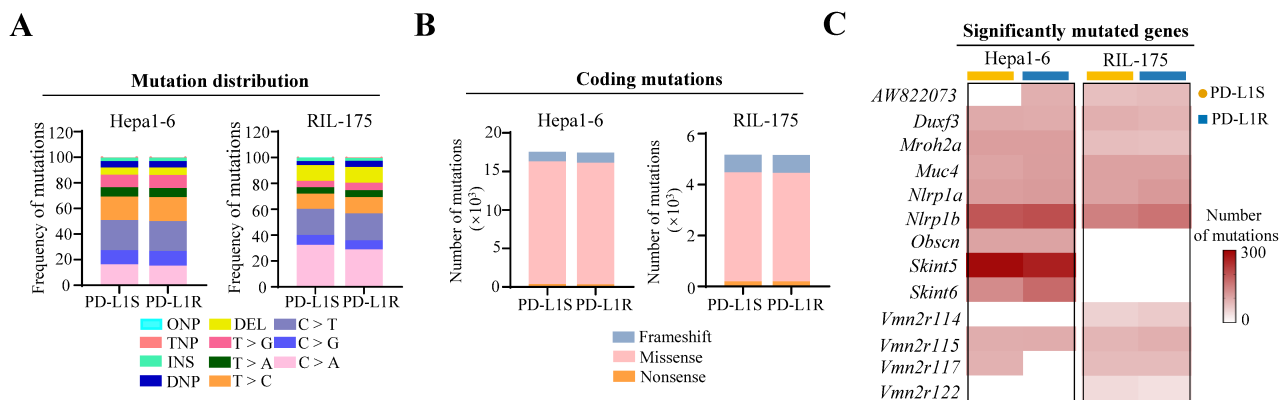
Supplemental material

BMJ Publishing Group Limited (BMJ) disclaims all liability and responsibility arising from any reliance placed on this supplemental material which has been supplied by the author(s)

Gut

Supplementary Figure 7. Mutation profiles of anti-PD-L1-sensitive and -resistant tumor cells.

(A) Distribution of different variant types (ONP, oligo-nucleotide polymorphism; TNP, triple nucleotide polymorphism; INS, insertion; DNP, double nucleotide polymorphism; DEL, deletion) and **(B)** distribution of coding mutations (frameshift, missense and nonsense) across Hepa1-6 or RIL-175 PD-L1S and PD-L1R cell lines. **(C)** Heatmap showing matrix of top 10 frequently mutated genes in Hepa1-6 or RIL-175 PD-L1S and PD-L1R cell lines.
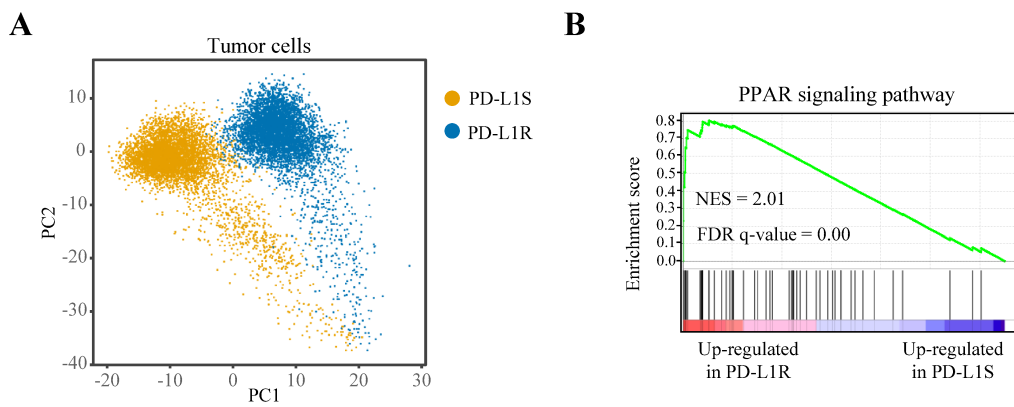
Supplementary Figure 8. Single-cell analysis of anti-PD-L1-sensitive and -resistant tumor cells.

(A) ScRNA-seq analysis of Hepa1-6 PD-L1S and PD-L1R tumor cell lines (n = 2). Principal component analysis (PCA) plots of the tumor cells are shown. **(B)** GSEA plot of PPAR signaling pathway (KEGG) in PD-L1R tumor cells compared to PD-L1S tumor cells. Consistent with the single-cell analysis from HCC tumor tissues **(figure 2A-C)**, the anti-PD-L1-resistant tumor cells showed distinctive transcriptional profile and significant enrichment of PPAR signaling pathway when compared to the initially-sensitive cells.

Supplemental material

BMJ Publishing Group Limited (BMJ) disclaims all liability and responsibility arising from any reliance placed on this supplemental material which has been supplied by the author(s)

Gut
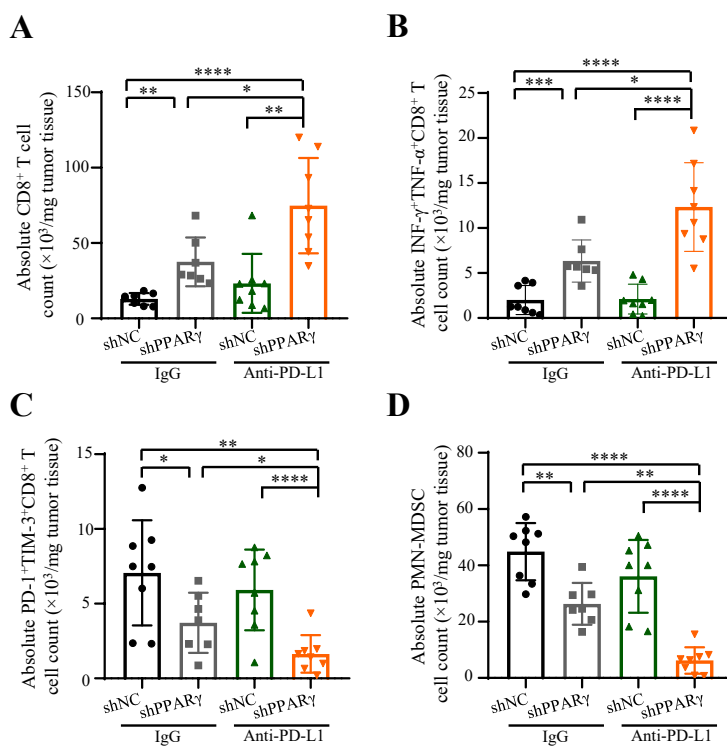
Supplementary Figure 9. Normalization of immune cell numbers to tumor size.

(A) Hepa1-6 PD-L1R-shNC or -shPPARγ tumor-bearing mice were treated with anti-PD-L1 10F.9G2 or isotype control LTF-2 as indicated in **figure 3A**. The absolute numbers ($\times 10^3$) of CD8$^+$ T cells, **(B)** IFN-γ$^+$TNF-α$^+$ cytotoxic CD8$^+$ T cells, **(C)** PD-1$^+$TIM-3$^+$ exhausted CD8$^+$ T cells, as well as **(D)** PMN-MDSCs in tumor tissues (mg) from indicated groups are shown (n = 7 to 8). Data represent as mean ± SD. Statistical significance was determined by unpaired two-tailed Student's t-test. *$P <$ 0.05; **$P <$ 0.01; ***$P <$ 0.001; ****$P <$ 0.0001.

Supplemental material

BMJ Publishing Group Limited (BMJ) disclaims all liability and responsibility arising from any reliance placed on this supplemental material which has been supplied by the author(s)

Gut
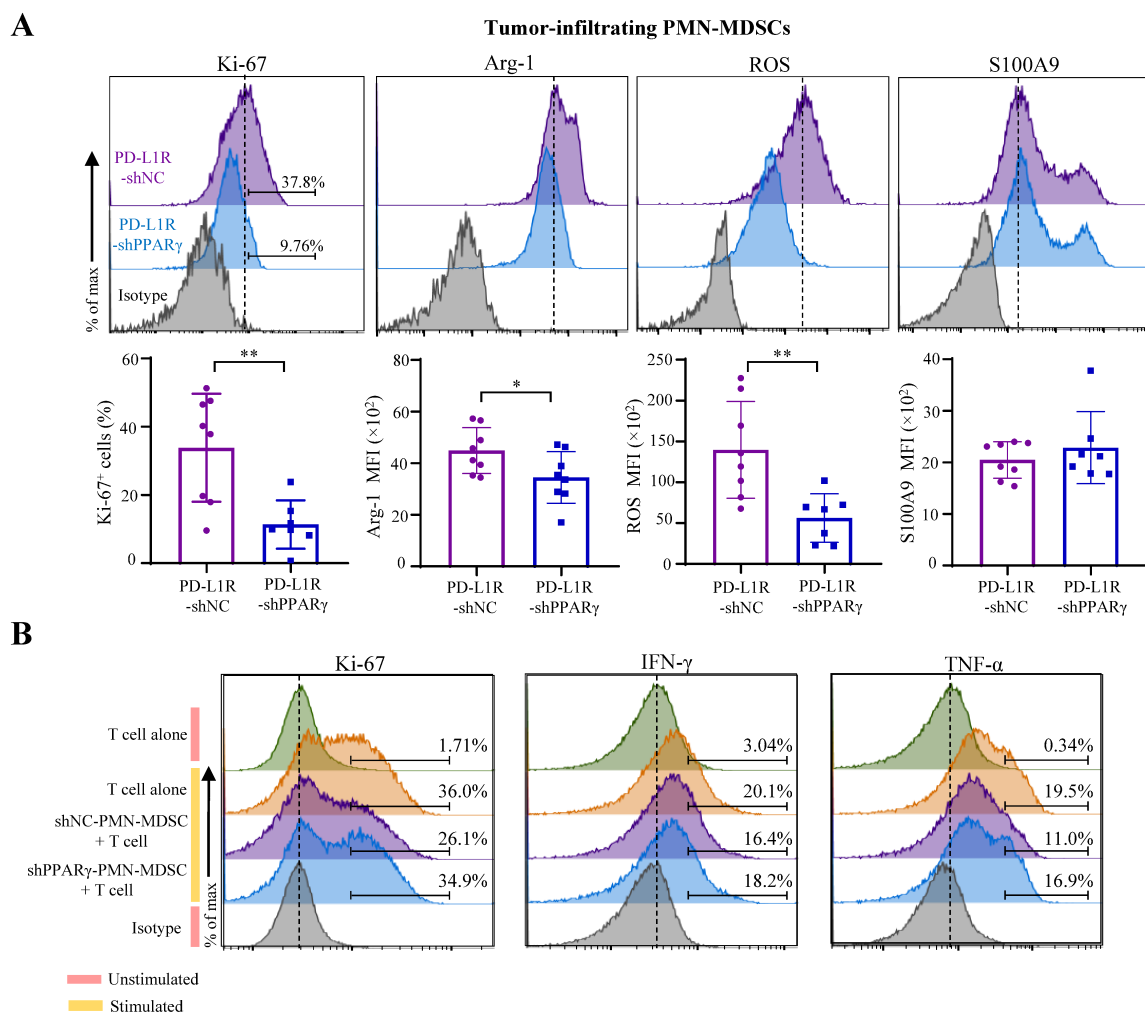
Supplementary Figure 10. Effects of tumoral PPARγ knockdown in immunosuppressive functions of PMN-MDSCs.

(A) Representative overlay histogram and proportions of proliferating Ki-67+ PMN-MDSCs, and expression levels (MFI) of Arg-1, ROS, as well as S100 calcium-binding protein A9 (S100A9) in PMN-MDSCs from Hepa1-6 PD-L1R-shNC or -shPPARγ tumor-bearing mice (n = 7 to 8). **(B)** Representative overlay histogram of Ki-67, IFN-γ and TNF-α in splenic CD8+ T cells co-cultured with PMN-MDSCs (1:1) from PPARγ-KD or control tumors. CD8+ T cells with or without stimulation with CD3/CD28 dynabeads and mouse recombinant IL-2 were served as positive or negative controls, respectively (n = 2). Dash line indicates the peak of the unstimulated T cell alone sample. Data represent as mean ± SD. Statistical significance was determined by unpaired two-tailed Student's t-test. $*P < 0.05$; $**P < 0.01$.
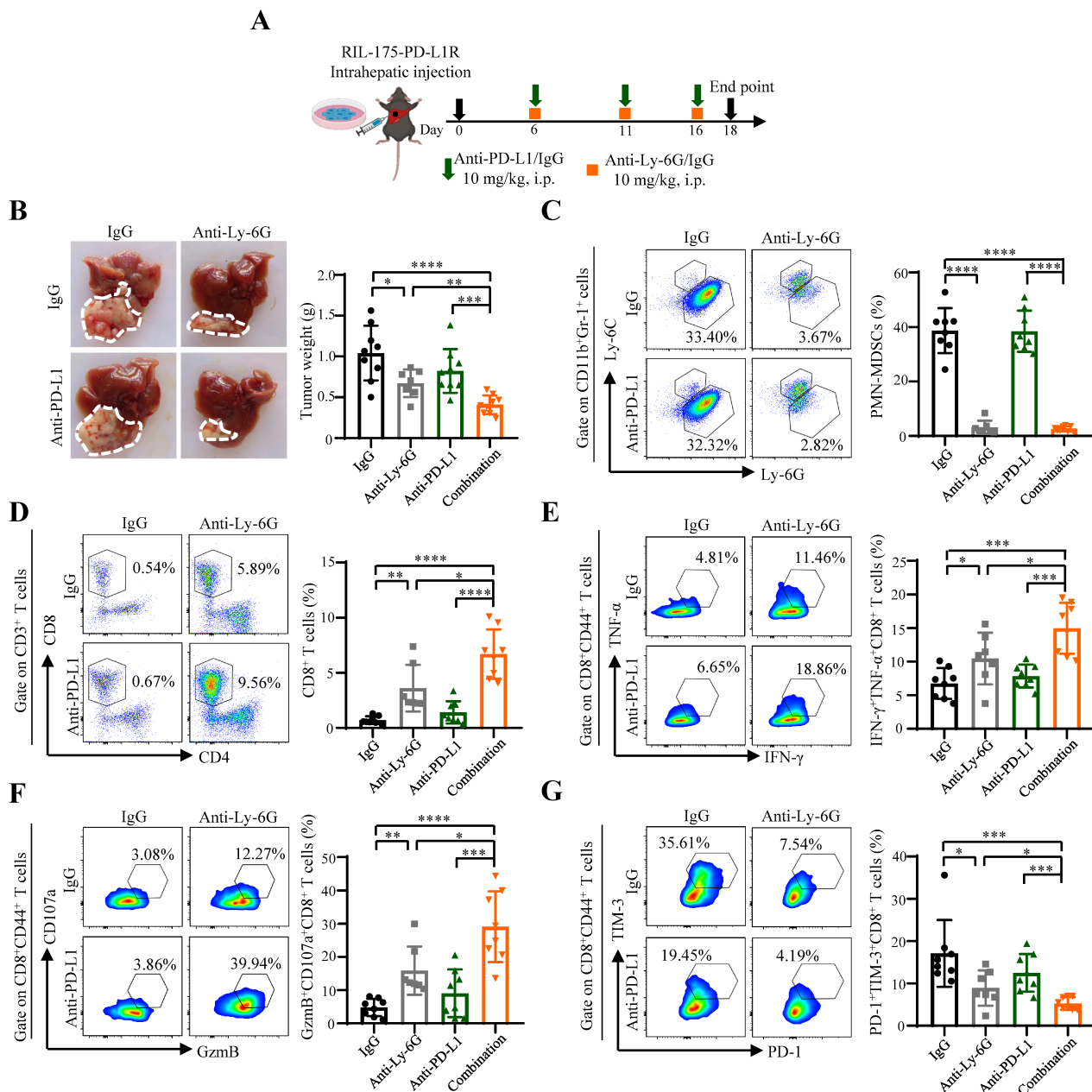
Supplementary Figure 11. MDSC depletion sensitizes resistant tumors to anti-PD-L1 treatment.

(A) Combination treatment schedule of anti-Ly-6G (1A8) and anti-PD-L1 antibody (10F.9G2) in mice bearing RIL-175 PD-L1R tumors. **(B)** Representative liver tumor photos and tumor weights of indicated groups (n = 7 to 9). **(C)** Representative flow cytometry dot plots and proportions of PMN-MDSCs and **(D)** CD8+ T cells in tumoral CD45+ cells, **(E)** CD44+IFN-γ+TNF-α+ cells, **(F)** CD44+GzmB+CD107a+ cells, and **(G)** CD44+PD-1+TIM-3+ cells in tumoral CD8+ T cells from indicated groups are shown (n = 7 to 8). Data represent as mean ± SD. Statistical significance was determined by unpaired two-tailed Student's t-test. *P < 0.05; **P < 0.01; ***P < 0.001; ****P < 0.0001.

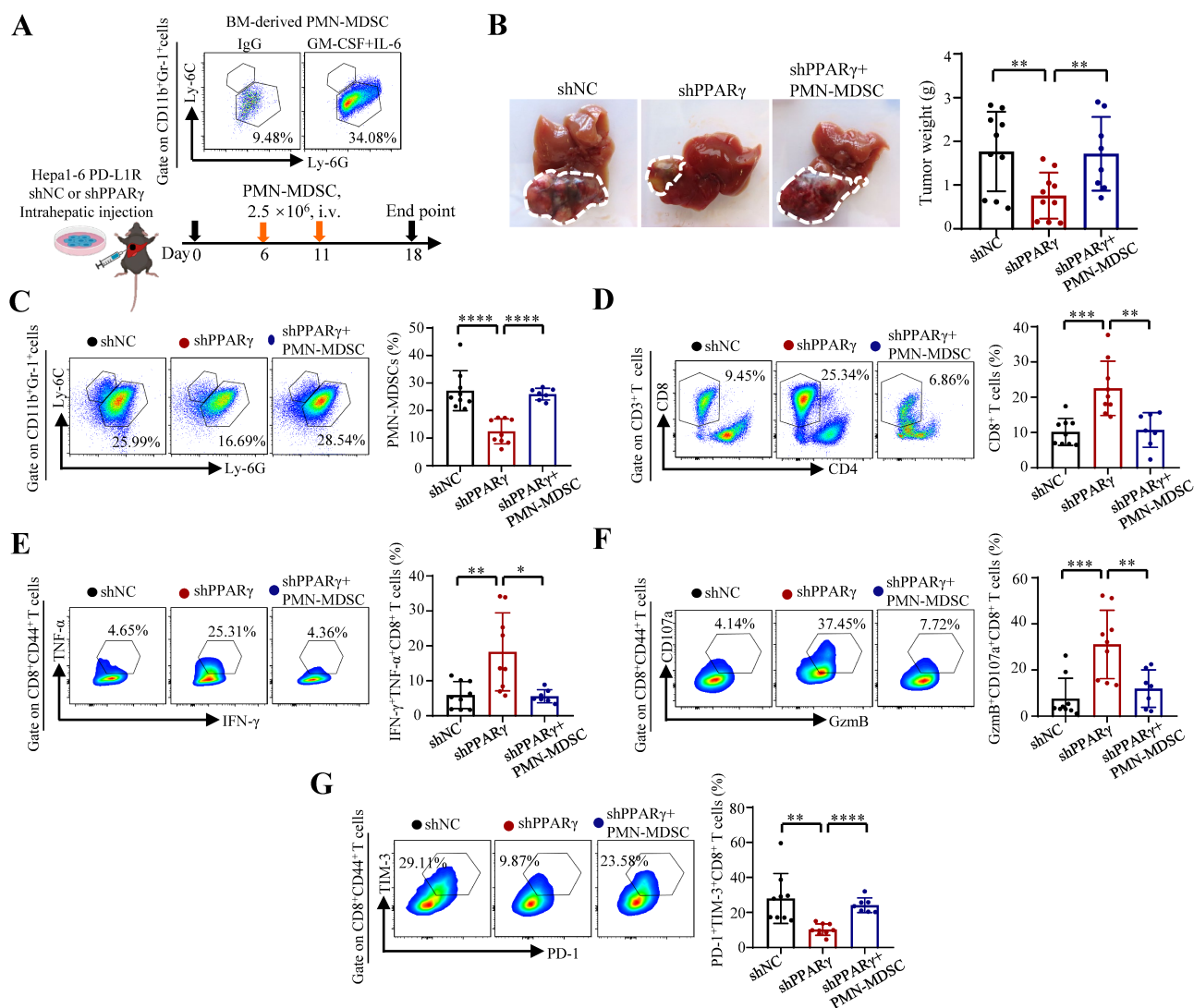**Supplementary Figure 12. Adoptive transfer of PMN-MDSCs abolishes TME reprograming and tumor regression by PPARγ knockdown.**

(A) PMN-MDSCs were induced from C57BL/6 naïve mouse-derived bone marrow (BM) cells in the presence of 40 ng/mL granulocyte macrophage colony-stimulating factor (GM-CSF) and IL-6 for 5 days. BM-PMN-MDSCs were confirmed by flow cytometry (top) and then purified by anti-Ly-6G microbeads and transferred intravenously into Hepa1-6 PD-L1R-shPPARγ tumor-bearing mice at day 6 and 11-post tumor inoculation. Mice were sacrificed at day 18 or humane end point (bottom). **(B)** Representative liver tumor photos and tumor weights of indicated groups (n = 8 to 10). **(C)** Representative flow cytometry dot plots and proportions of PMN-MDSCs and **(D)** CD8$^+$ T cells in tumoral CD45$^+$ cells, **(E)** CD44$^+$IFN-γ$^+$TNF-α$^+$ cells, **(F)** CD44$^+$GzmB$^+$CD107a$^+$ cells, and **(G)** CD44$^+$PD-1$^+$TIM-3$^+$ cells in tumor CD8$^+$ T cells from indicated groups are shown (n = 7 to 9). Data represent as mean ± SD. Statistical significance was determined by unpaired two-tailed Student's t-test. *$P < 0.05$; **$P < 0.01$; ***$P < 0.001$; ****$P < 0.0001$.

Supplemental material

BMJ Publishing Group Limited (BMJ) disclaims all liability and responsibility arising from any reliance placed on this supplemental material which has been supplied by the author(s)

Gut
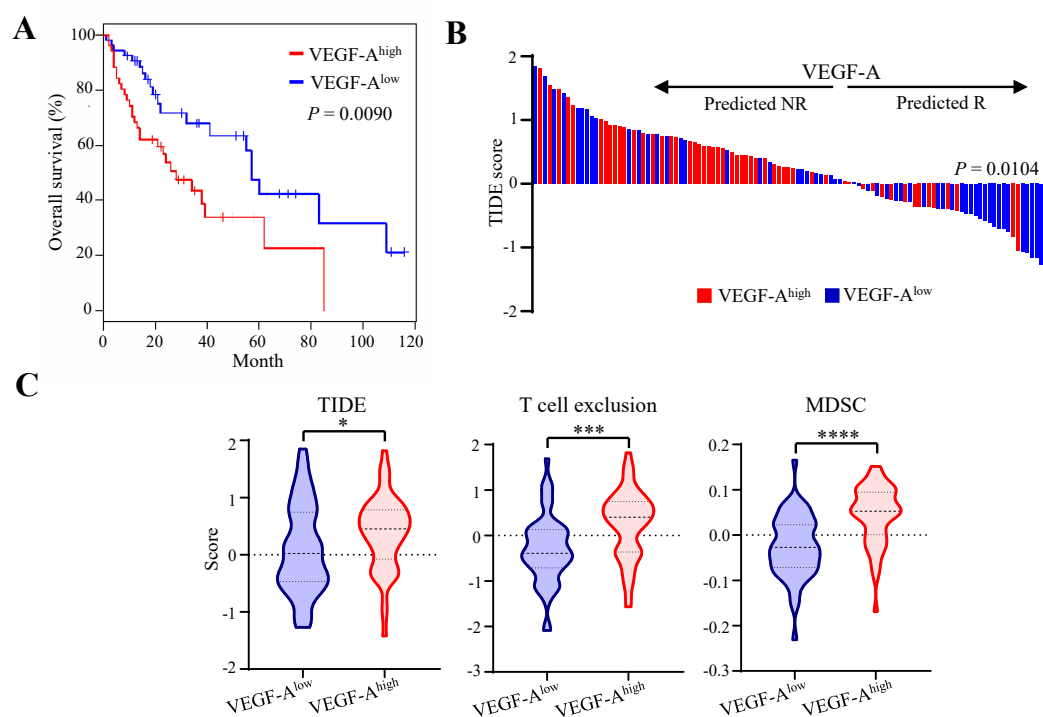
Supplementary Figure 13. Association between VEGF-A expression with overall survival and predicted ICB response in HCC patients from TCGA dataset.

(A) TCGA HCC samples with high (n = 55) and low (n = 55) mRNA levels of *VEGFA* was stratified by top and bottom 15% in 369 patients. Kaplan-Meier curves of overall survival in HCC patients according to the expression of *VEGFA*. **(B)** Prediction of potential clinical ICB response in VEGF-A^{high} versus VEGF-A^{low} HCC patients using the TIDE signature. **(C)** Analysis of TIDE, T cell exclusion and MDSC scores by TIDE algorithm in VEGF-A^{high} and VEGF-A^{low} HCC patients. Statistical significance was assessed by two-sided log-rank (Mantel-Cox) test for (A), two-sided Chi-square test for (B), and unpaired two-tailed Student's t-test for (C). *$P < 0.05$; ***$P < 0.001$; ****$P < 0.0001$.
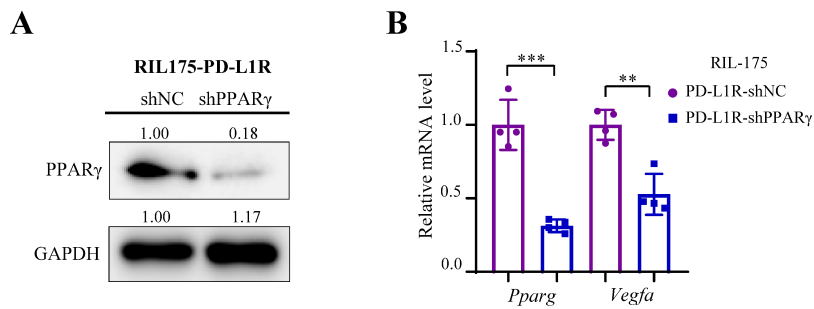
Supplementary Figure 14. Effect of PPARγ knockdown on VEGF-A expression in anti-PD-L1-resistant tumor cells.

(A) Representative western blot image of PPARγ in RIL-175 PD-L1R-shNC and -shPPARγ tumor cell lines. GAPDH served as loading control. **(B)** Relative mRNA levels of *Pparg* and *Vegfa* in RIL-175 PD-L1R-shNC and -shPPARγ cells (n = 4) as determined by RT-qPCR. Data are normalized to basal levels. Statistical significance was determined by unpaired two-tailed Student's t-test. **$P <$ 0.01; ***$P <$ 0.001.
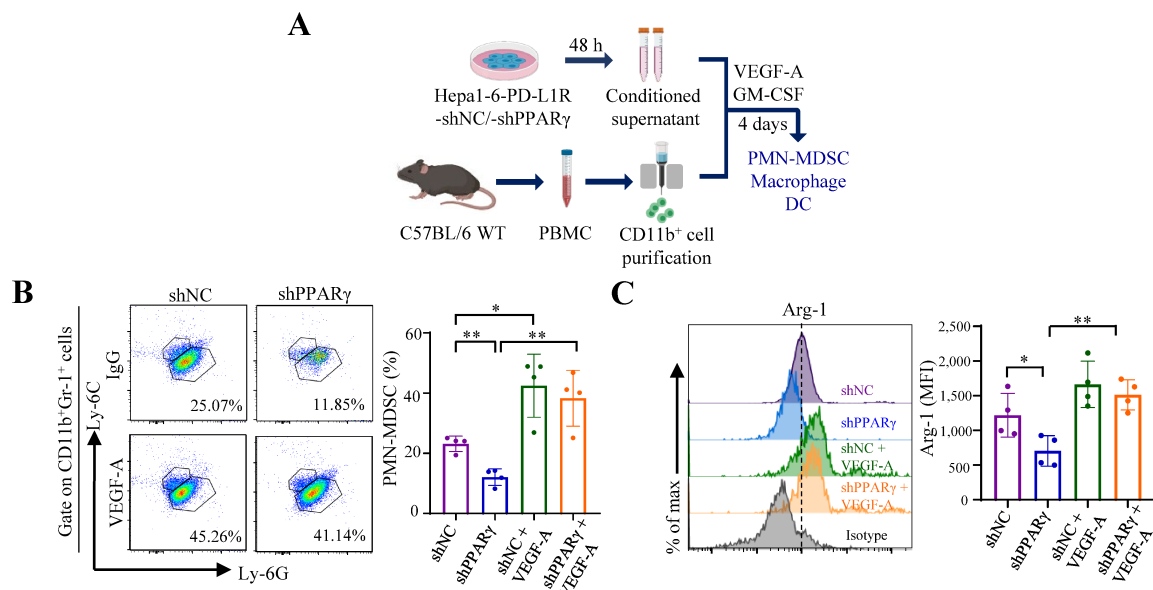
Supplementary Figure 15. PPARγ-expressing tumor cell-derived VEGF-A mediates MDSC expansion from peripheral blood mononuclear cells.

(A) Schematic illustration of *ex vivo* myeloid cell functional assay. **(B)** Representative flow cytometry dot plots and proportions of PMN-MDSCs in CD45$^+$ cells in indicated groups (n = 4). **(C)** Representative overlay histogram and expression levels determined by MFI of Arg-1 in PMN-MDSCs (n = 4). Dash line indicates the peak of sample treated with conditional media (CM) of Hepa1-6 PD-L1R-shNC cells. Data represent as mean ± SD. Statistical significance was determined by unpaired two-tailed Student's t-test. *$P < 0.05$; **$P < 0.01$.

Supplemental material

BMJ Publishing Group Limited (BMJ) disclaims all liability and responsibility arising from any reliance placed on this supplemental material which has been supplied by the author(s)

Gut
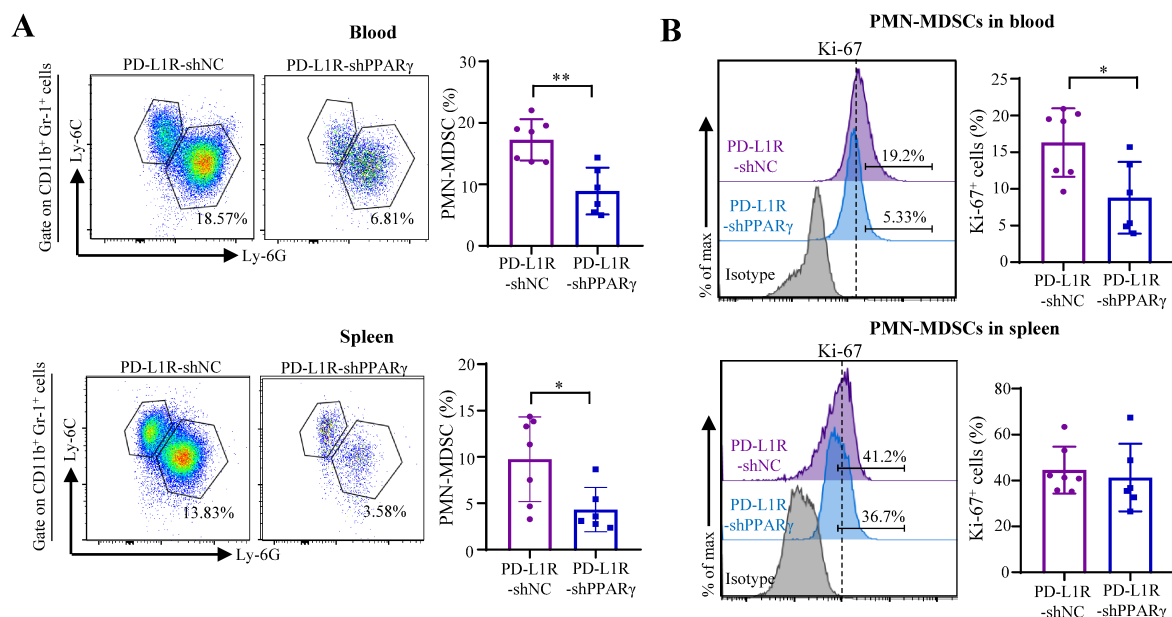
Supplementary Figure 16. Effects of tumoral PPARγ knockdown in the frequency of PMN-MDSCs in blood and spleen of tumor-bearing mice.

(A) Representative flow cytometry dot plots and proportions of PMN-MDSCs in blood and spleen of Hepa1-6 PD-L1R-shNC or -shPPARγ tumor-bearing mice. **(B)** Representative overlay histogram and proportions of proliferating Ki-67^{+} PMN-MDSCs in blood and spleen in Hepa1-6 PD-L1R-shNC or -shPPARγ tumor-bearing mice as determined by flow cytometry (n = 6 to 7). Dash line indicates the peak of the PD-L1R-shNC sample. Data represent as mean ± SD. Statistical significance was determined by unpaired two-tailed Student's t-test. *$P < 0.05$; **$P < 0.01$.

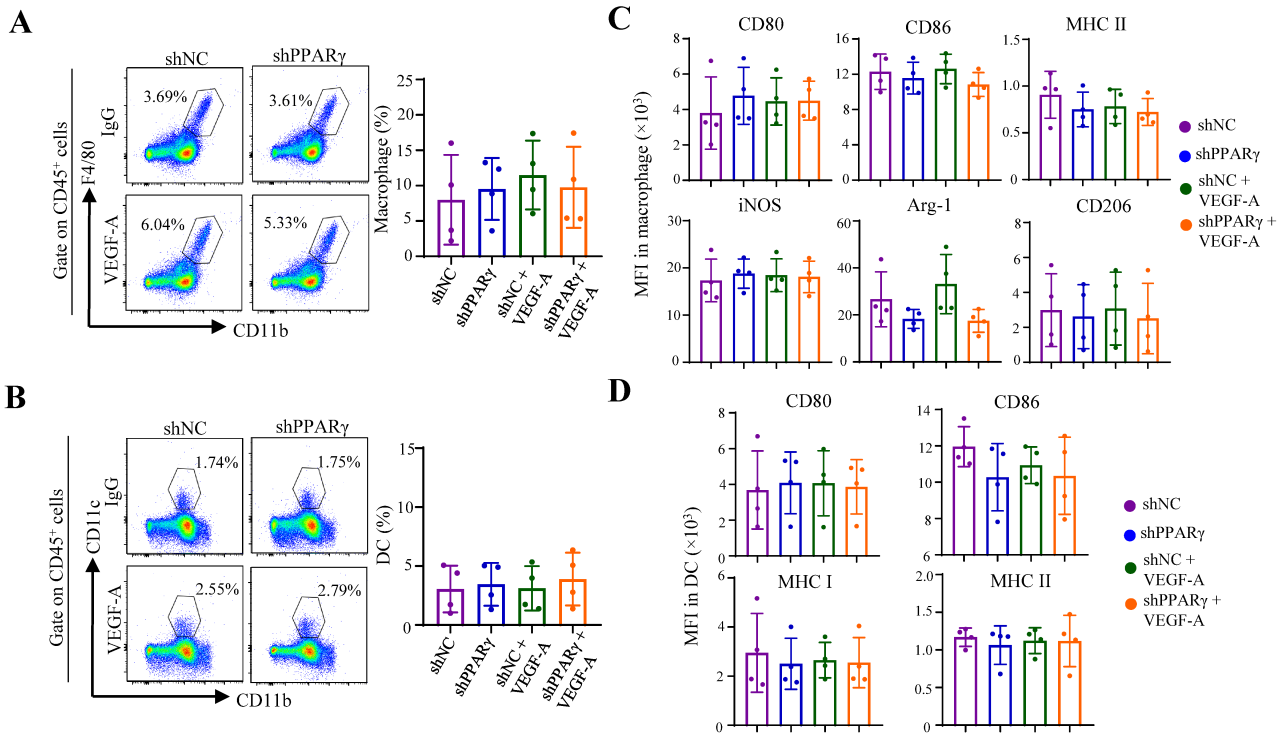**Supplementary Figure 17. PPARγ-expressing tumor cell-derived VEGF-A has limited effect on the proportions and phenotypes of macrophages and DCs in blood.**

Ex vivo myeloid cell functional assay was performed as in **supplementary figure 15A**. **(A)** Representative flow cytometry dot plots and proportions of macrophages and **(B)** DCs in CD45$^+$ cells (n = 4). **(C)** Expression levels determined by MFI of CD80, CD86, MHC II, iNOS, Arg-1, and CD206 in macrophages and **(D)** CD80, CD86, MHC I and MHC II in DCs (n = 4). Data represent as mean ± SD. Statistical significance was determined by unpaired two-tailed Student's t-test.

Supplemental material

BMJ Publishing Group Limited (BMJ) disclaims all liability and responsibility arising from any reliance placed on this supplemental material which has been supplied by the author(s)

Gut

Supplementary Figure 18. VEGFR2 expressions on PMN-MDSCs and CD8+ T cells in anti-PD-L1-resistant tumors.

(A) Representative overlay histogram, proportion and MFI of VEGFR2 in PMN-MDSCs and (B) CD8+ T cells from Hepa1-6 PD-L1R-shNC or shPPARγ tumor-bearing mice were assessed by flow cytometry (n = 7). Dash line indicates the peak of the PD-L1R-shNC sample. Data represent as mean ± SD. Statistical significance was determined by unpaired two-tailed Student's t-test.

Supplemental material

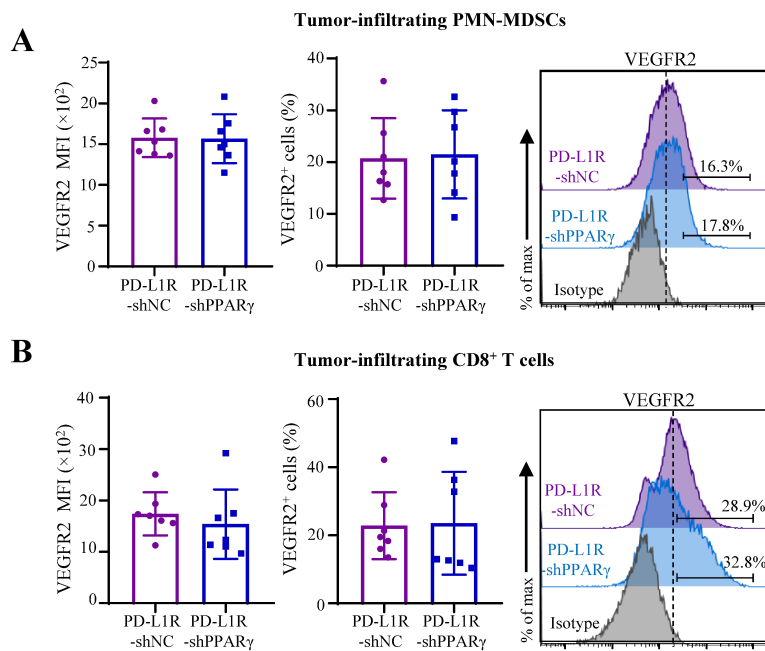BMJ Publishing Group Limited (BMJ) disclaims all liability and responsibility arising from any reliance placed on this supplemental material which has been supplied by the author(s)

Gut

Supplemental material

BMJ Publishing Group Limited (BMJ) disclaims all liability and responsibility arising from any reliance placed on this supplemental material which has been supplied by the author(s)

Gut

Supplementary Figure 19. Tumor cell-intrinsic PPARγ or VEGF-A inhibition reverts immunosuppression and ICB resistance.

(A) Treatment schedule for anti-PD-L1 antibody (10F.9G2) or isotype control (LTF-2) in RIL-175 PD-L1R-shNC, -shVEGF-A or -shPPARγ-tumor bearing mice (top). Relative mRNA level of *Vegfa* in RIL-175 PD-L1R-shNC and –shVEGF-A cells (n = 3) as determined by RT-qPCR (bottom). Data are normalized to basal levels. **(B)** Representative liver tumor photos and tumor weights of PD-L1R-shNC-, -shVEGFA- or -shPPARγ-tumor bearing mice treated with anti-PD-L1 or isotype control at the endpoint are shown (n = 9 to 10). **(C)** Representative flow cytometry dot plots, proportions, and absolute numbers of CD8$^+$ T cells, **(D)** CD44$^+$GzmB$^+$CD107a$^+$ cytotoxic CD8$^+$ T cells, **(E)** CD44$^+$PD-1$^+$TIM-3$^+$ exhausted CD8$^+$ T cells, as well as **(F)** PMN-MDSCs in indicated tumors (n = 8 to 9). Data represent as mean ± SD. Statistical significance was determined by unpaired two-tailed Student's t-test. *$P < 0.05$; **$P < 0.01$; ***$P < 0.001$; ****$P < 0.0001$.
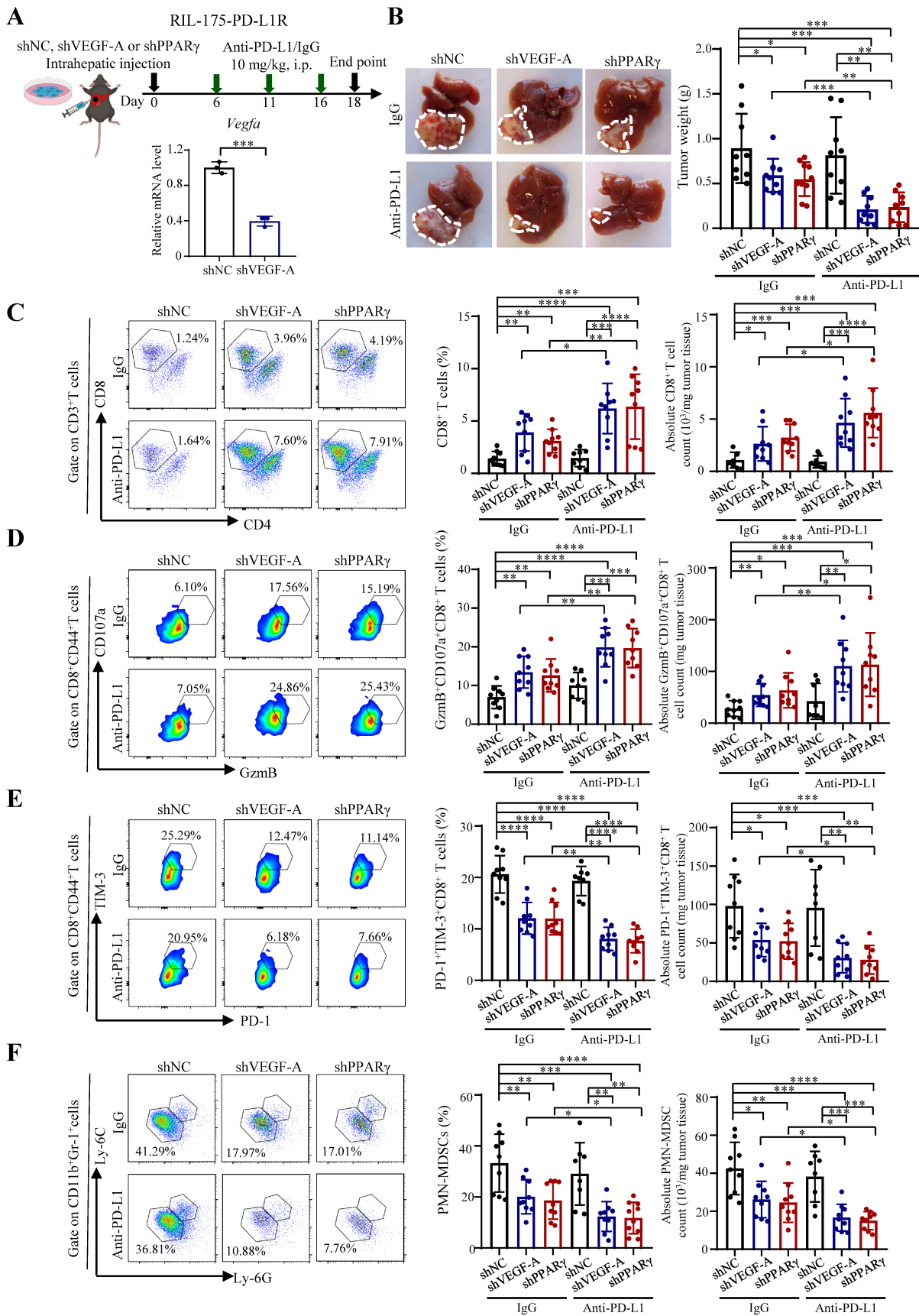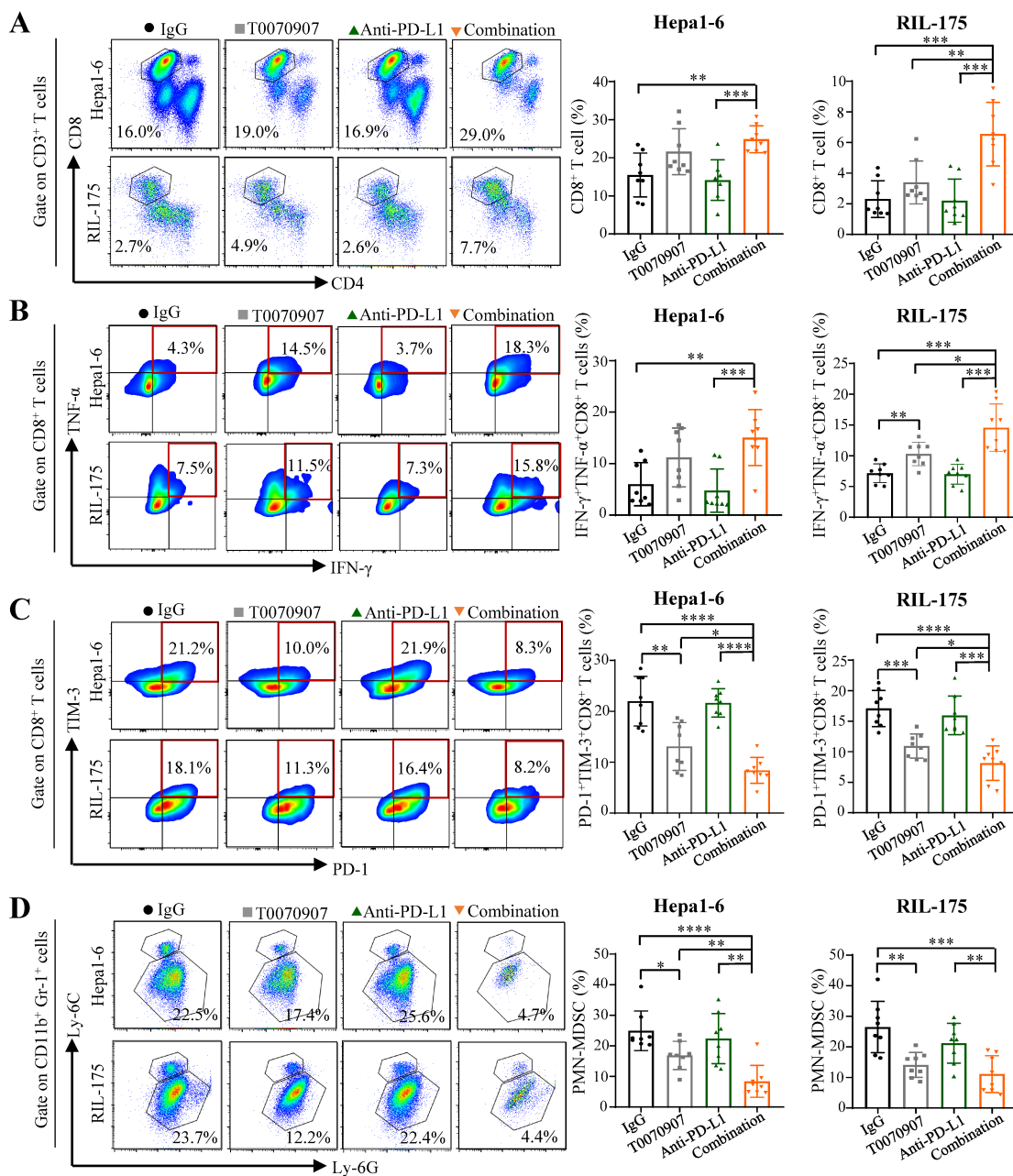
Supplementary Figure 20. Immune profiling of anti-PD-L1-resistant models upon treatment with single or combined PPARγ antagonist and anti-PD-L1 antibody.

(A) Hepa1-6 or RIL-175 PD-L1R tumor-bearing mice were treated with vehicle control, T0070907, anti-PD-L1 or T0070907 and anti-PD-L1 as indicated in **figure 5A**. Representative flow cytometry dot plots and proportions of CD8+ T cells in CD45+ cells, **(B)** IFN-γ+TNF-α+ or **(C)** PD-1+TIM-3+ cells in CD8+ T cells, as well as **(D)** PMN-MDSCs in CD45+ cells from Hepa1-6 (n = 8) or RIL-175 PD-L1R tumors (n = 8). Data represent as mean ± SD. Statistical significance was determined by unpaired two-tailed Student's t-test. * *P* < 0.05; ** *P* < 0.01; *** *P* < 0.001; **** *P* < 0.0001.
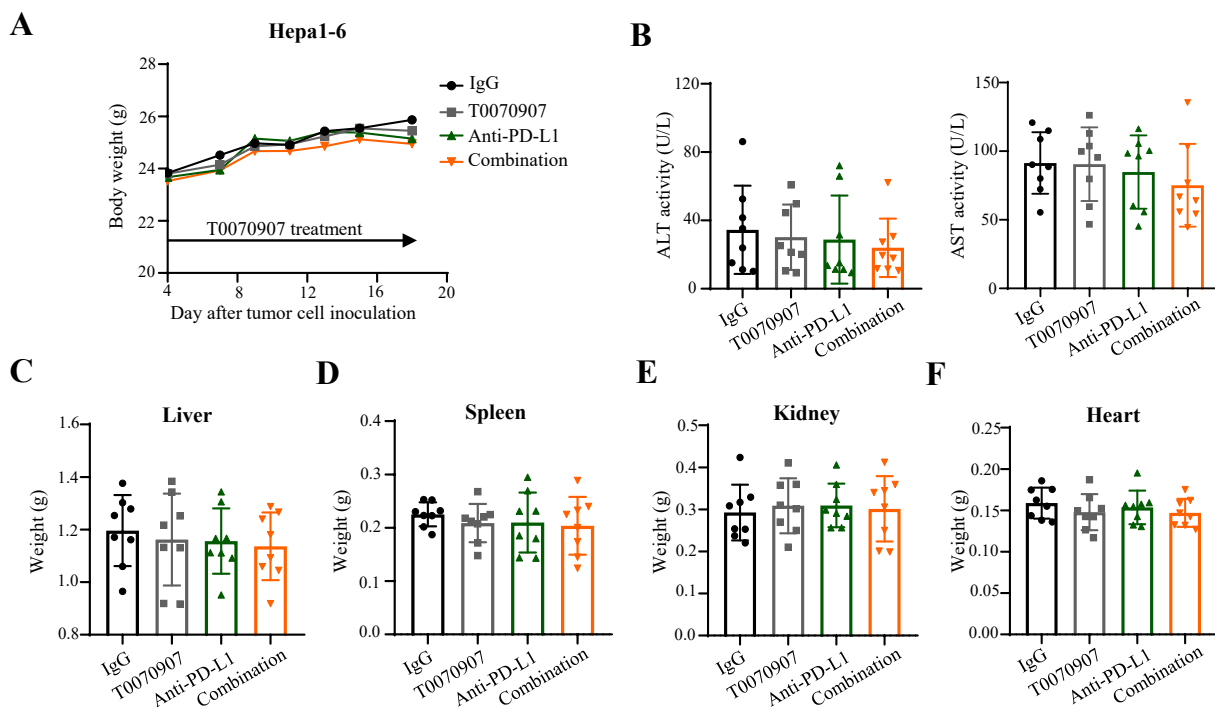
Supplementary Figure 21. Evaluation of toxicity in anti-PD-L1-resistant model upon treatment with single or combined PPARγ antagonist and anti-PD-L1 antibody.

(A) Hepa1-6-PD-L1R tumor-bearing mice were treated with vehicle control, T0070907, anti-PD-L1 or T0070907 and anti-PD-L1 as indicated in **figure 5A**. Body weights of the four indicated groups at different time points were shown (n = 8). **(B)** Serum levels of alanine aminotransferase (ALT) and aspartate aminotransferase (AST) in indicated groups were shown (n = 8). **(C)** Weights of liver, **(D)** spleen, **(E)** kidney, and **(F)** heart of the indicated treatment groups (n = 8). Data represent as mean ± SD. Statistical significance was determined by unpaired two-tailed Student's t-test.
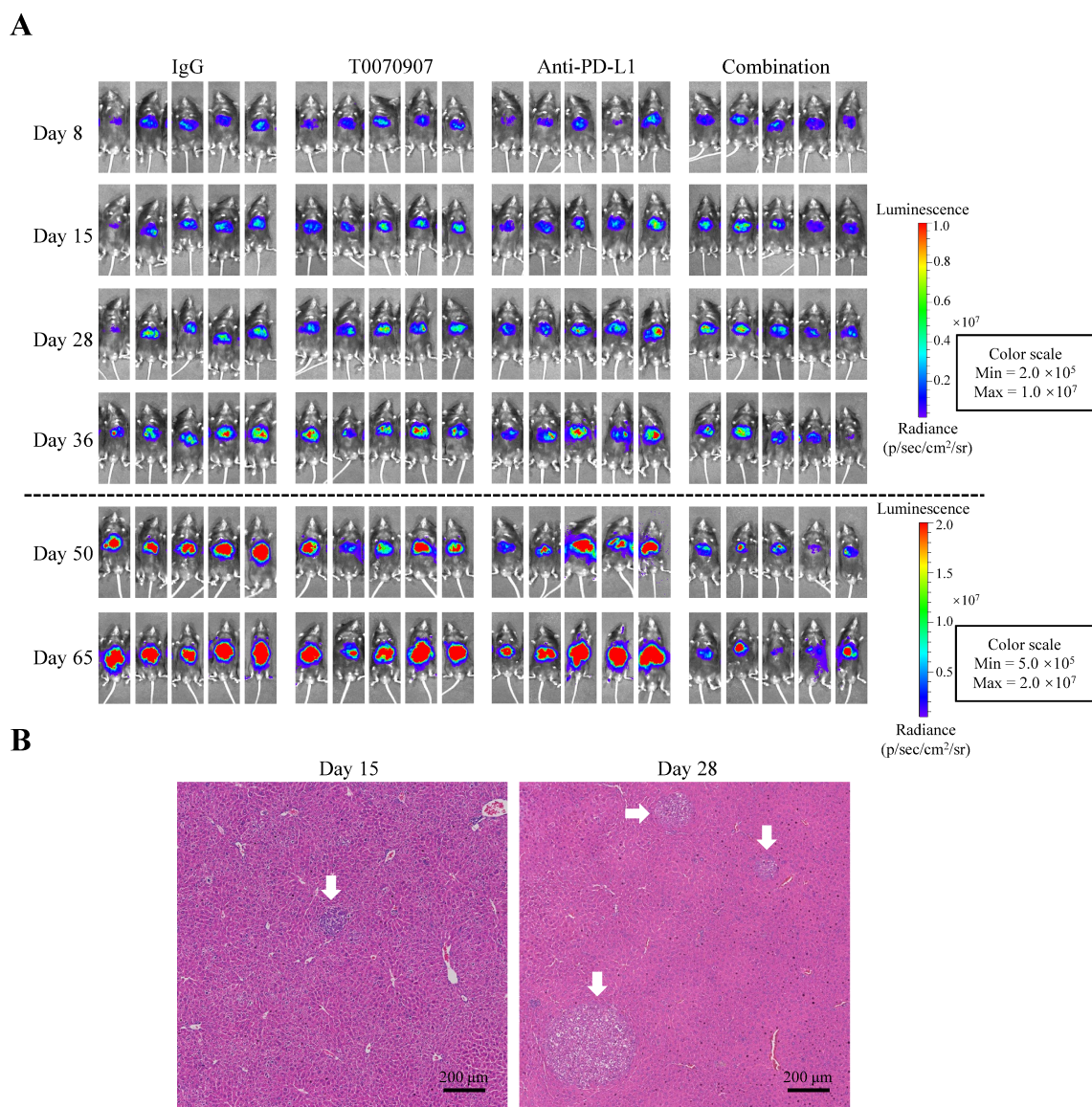
Supplementary Figure 22. Monitoring of N-Ras/c-Myc-induced HCC model upon treatment with single or combined PPARγ antagonist and anti-PD-L1 antibody.

(A) Representative *in vivo* bioluminescence images of N-Ras/c-Myc-tumor bearing mice treated with anti-PD-L1 and/or T0070907 at indicated time points are shown. **(B)** Representative H&E staining images of the N-Ras/c-Myc-induced HCC model (isotype control) at day 15 (left) and day 28 (right) post-HDTVi are shown. White arrow indicates the tumor nodule. Scale bars, 200 μm.

Supplemental material

BMJ Publishing Group Limited (BMJ) disclaims all liability and responsibility arising from any reliance placed on this supplemental material which has been supplied by the author(s)

Gut
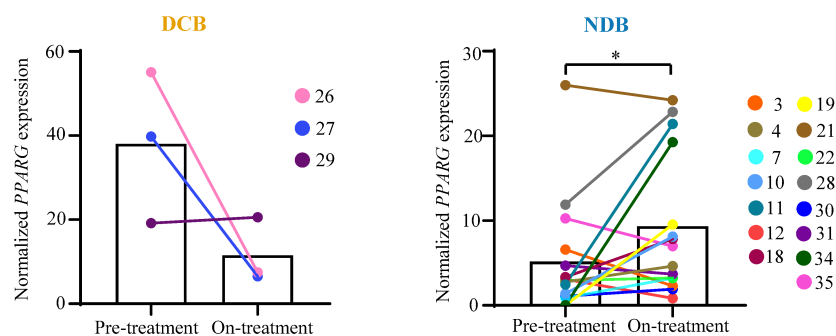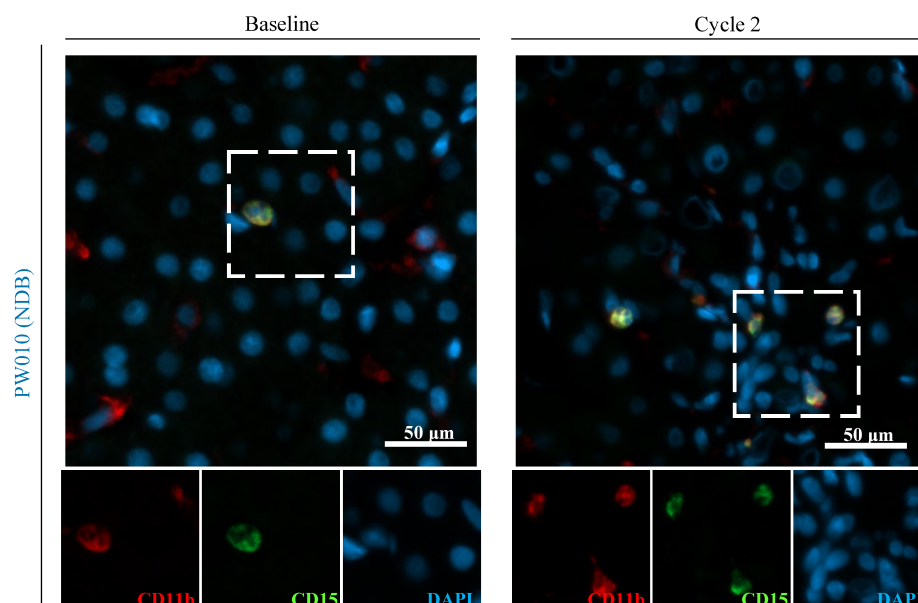
Supplementary Figure 23. Determination of PPARγ expression and PMN-MDSC in patients undergone anti-PD-1 therapy.

(A) Normalized *PPARG* expression in tumor cells from paired pre- and on-treatment samples in patients with durable clinical benefits (DCB; left) and non-durable benefit (NDB; right). Patient IDs are indicated with different colors. **(B)** Representative co-immunofluorescence images of PMN-MDSC markers CD11b (red) and CD15 (green), and nuclei marker DAPI of paired pre- and on-treatment biopsies from PW010 (NDB) are shown. Scale bars, 50 μm. Data represent as mean. Statistical significance was determined by paired two-tailed Student's t-test. *$P < 0.05$.

A

$R = 0.6469$
$P < 2.2 \times 10^{-16}$
$n = 3041$ cells

B

$R = 0.6106$
$P < 2.1 \times 10^{-10}$
$n = 89$ cells
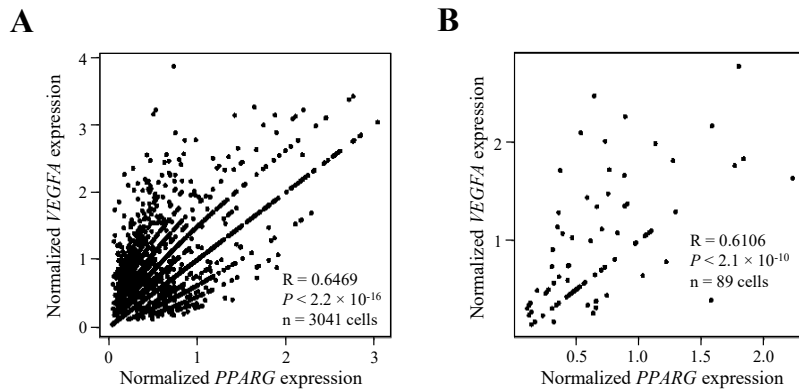
Supplementary Figure 24. Correlation between PPARG and VEGFA expressions in tumor cells of HCC patients.

Positive correlations between PPARG and VEGFA expressions in tumor cells of (A) our in-house and (B) a public[1] dataset of human liver cancer scRNA-seq. Each dot represents an individual tumor cell. Tumor cells with non-zero expression levels of PPARG and VEGFA were included in this analysis. Two-tailed Pearson's correlation was used to describe the correlation between variables.

Supplemental material

BMJ Publishing Group Limited (BMJ) disclaims all liability and responsibility arising from any reliance placed on this supplemental material which has been supplied by the author(s)

Gut

Supplementary Methods

Cell lines. Hepa1-6 (ATCC, CRL-1830) and RIL-175 (generous gift from Prof. Lars Zender and Prof. Tim Greten) were used. All cell lines were cultured in Dulbecco's Modified Eagle's Medium (DMEM, Gibco), supplemented with 10% Fetal Bovine Serum (FBS, Gibco) in a 37°C humidified chamber with 5% CO_2.

***In vivo* selection of immunotherapy-resistant HCC cell lines.** To select anti-PD-L1 therapy resistant (PD-L1R) HCC cells, Hepa1-6 and RIL-175 HCC orthotopic mouse models were first established via parental immunotherapy-sensitive HCC cell lines (PD-L1S) as previously described[2 3]. In brief, 5×10^6 Hepa1-6 or 5×10^5 RIL-175 PD-L1S cells were injected into left liver lobe of 7-8-week-old male C57BL/6 mice, followed by intraperitoneal injection (i.p.) of anti-PD-L1 antibody (clone 10F.9G2, 10 mg/kg; BioXcell) at day 6, 11 and 16 post-tumor inoculation. Mice were sacrificed at day 18 and the residual tumor cells were excised for single cell isolation. After 2 weeks of *ex vivo* culture, the tumor cells were re-inoculated into a new recipient mouse. As a result of 6-7 cycles of *ex vivo* selection, the tumor cells that displayed resistance to anti-PD-L1 antibody were collected and referred as Hepa1-6 or RIL-175-PD-L1R cells. Cells were then passed and cultured in standard condition.

Construction of PPARγ- and VEGF-A-knockdown (KD) stable cell lines. pGLVH1-GFP-Puro lentiviral vector encoding short hairpin RNA (shRNA) against for mouse PPARγ (GGATGTCTCACAATGCCATCA), VEGF-A (CAAGATCCGCAGACGTGTAAA) or a scrambled sequence as negative control (NC) (GTTCTCCGAACGTGTCACGT) were purchased from GenePharma. Lentivirus was generated as previously[4] and infected Hepa1-6 or RIL-175 PD-

L1R cells, followed by 2-week *in vitro* selection via culturing under 2 µg/ml puromycin. mRNA and protein expressions of PPARγ and VEGF-A were determined by RT-qPCR and western blot.

***In vivo* studies.** To investigate the cellular and molecular mechanisms of ICB resistant, PD-L1S and PD-L1R cells generated from Hepa1-6 (5×10^6) or RIL-175 (5×10^5) were intrahepatically injected into left liver lobe of male C57BL/6 mice. An additional model in immunodeficient BALB/c nude mice by inoculation of Hepa1-6 (5×10^6) or RIL-175 (5×10^5) PD-L1S and PD-L1R cells were established in parallel to determine the role of adaptive immune response in ICB resistance. Mice were then treated with anti-PD-L1 or isotype control (clone LTF.2, 10 mg/kg; BioXcell) antibodies via i.p. injection at day 6, 11, and 16. Blood, spleen and tumor were collected for primary cell isolation and subsequent immune profiling analysis by multi-color flow cytometry as well as for scRNA-seq, western blot and ELISA.

To study the tumor-intrinsic PPARγ or VEGF-A in determining ICB resistance, groups of male C57BL/6 mice were intrahepatically inoculated with PD-L1R-shNC, -shPPARγ or -shVEGF-A cells, followed by anti-PD-L1 or isotype control antibody treatment as described above. To investigate the role of PMN-MDSCs in ICB resistance, RIL-175 PD-L1R orthotopic tumor-bearing mice were treated with anti-Ly-6G antibody (clone 1A8, 10 mg/kg; BioXcell) alone or in combination with anti-PD-L1 antibody via i.p. injection at day 6, 11, and 16. For PMN-MDSC adoptive transfer, bone marrow cells were collected from naïve C57/BL6 mice and plated at 1×10^6 cells/mL in RPMI1640 medium plus 10% fetal bovine serum, 0.1% penicillin and streptomycin, and stimulated with 40 ng/mL granulocyte macrophage colony-stimulating factor (GM-CSF) and IL-6 at 37°C at 10% CO_2 for 5 days. PMN-MDSCs were purified using anti-Ly-

6G microbeads (Miltenyi Biotec) and intravenously injected (2.5×10^6) into Hepa1-6 PD-L1R-shNC or -shPPARγ tumor-bearing mice at day 6 and 11-post tumor inoculation. To determine the therapeutic potential of PPARγ inhibition in overcoming ICB resistance, Hepa1-6 and RIL-175 PD-L1R orthotopic tumor-bearing mice were treated with T0070907 (2 mg/kg; Selleckchem) alone or in combination with anti-PD-L1 antibody. T0070907 or PBS was administrated via i.p injection daily, while anti-PD-L1 or isotype control antibodies were administrated via i.p injection at day 6, 11 and 16. All mice were euthanized at day 18 post-tumor cell inoculation or at endpoints approved by CUHK-AEEC. The survival of treated mice was assessed for a period of 4 months. Tumor, liver, spleen, kidney and heart were weighted and analysed by immunohistochemistry staining and functional enzyme measurement to evaluation drug toxicity. Blood, spleen and tumor were collected for primary cell isolation and subsequent immune profiling analysis by multi-color flow cytometry as well as for ELISA.

To further investigate the therapeutic efficacy of the combinatory regimen, we employed an additional spontaneous HCC model induced by HDTVi of oncogenes together with the sleeping beauty transposase 13 (SB13) in C57BL/6 male mice. 20 µg pT3-EF1a-NRasV12, 10 µg pT3-EF1a-c-Myc-IRES-luciferase and 7.5 µg pCMV-SB13 were diluted in 2 ml sterile 0.9% NaCl, filtered through a 0.22-µm filter and injected at 0.1 ml/g body weight through the tail vein in 5-7 seconds as described previously[5]. The kinetics of tumor growth was monitored by bioluminescence *in vivo* imaging (IVIS spectrum system; PerkinElmer). Mice were then separated into four groups with equivalent luciferase signal and treated with T0070907 alone or in combination with anti-PD-L1 antibody starting at day 28 post-HDTVi as described above. All mice were euthanized at day 65 post-HDTVi or at endpoints approved by CUHK-AEEC. Tumor were collected for primary cell

isolation and subsequent immune profiling analysis by multi-color flow cytometry as well as for western blot. For histological examination, the liver tissue of each mouse with similar size from the same lobe of the liver was collected. After hematoxylin and eosin (H&E) staining, tumor burden was evaluated by liver weight/body weight (LW/BW), number and diameter of tumor nodules[5 6].

RNA-seq and data analysis. Total RNA was extracted from Hepa1-6 PD-L1S and PD-L1R cell lines using TRIzol (Invitrogen) and purified by RNeasy MinElute Cleanup Kit (Qiagen). RNA integrity and concentration were determined on 2100 Bioanalyzer (Agilent Technologies) and Qubit 2.0 (Thermo Fisher Scientific), respectively. Complementary DNA (cDNA) synthesis and library preparation were performed by NEBNext® Ultra II Directional RNA Library Prep Kit (Illumina) according to the manufacturer's instructions. Flowcell cluster amplification and sequencing were performed using Illumina NovaSeq 6000 system. Paired-end reads (100-bp) were pseudo-aligned to the mm10 reference genome for abundance quantification using kallisto v0.44.0[7]. Differential expression analysis was performed using DESeq2[8].

Whole-exome sequencing (WES) and data analysis. Genomic DNA was isolated from Hepa1-6 PD-L1S and PD-L1R cell lines using DNeasy Blood and Tissue Kit (Qiagen). Library construction and sequencing were performed by BGI Tech using SureSelect[XT] Mouse All Exon V6 Kit (Agilent Technologies) and NovaSeq 6000 System (Illumina). All raw data were aligned to the GRCm38 mouse genome using BWA tools (v0.7.17). The PCR duplicate reads were marked by Picard (v2.23.3). To generate analysis-ready BAM files, indel realignment and base recalibration were performed by Genome Analysis Toolkit (GATK, v4.1.9.0). Somatic mutation

calling and genetic variant annotation were performed by Mutect2 and SnpEff (v5.0e), respectively. Regarding copy number variant (CNV) analysis, CNVkit (v0.9.9) was applied to infer and visualize copy-number aberrations[9].

RNA extraction and RT-qPCR. Total RNA from tumor cell lines or tissues was extracted by using TRIzol (Invitrogen). The quality and quantity of total RNA were determined by measuring absorbance at 260 nm/280 nm using NanoDrop Spectrophotometer ND-2000 (NanoDrop Biotechnologies). 1 µg RNA was reverse transcribed to cDNA using Reverse Transcription Master Kit (Takara) according to the manufacturer's instructions. Quantitative real-time PCR (QPCR) was performed in triplicates by Power SYBR Green (SYBR® Premix Ex Taq™ II, Takara) and QuantStudio™ 7 Flex Real-Time PCR System (Applied Biosystems). *Glyceraldehyde-3-phosphate dehydrogenase* (*GAPDH*) was used as an internal control. Samples were run in technical triplicates. The sequences of primers are listed in the **supplementary table 2**.

Western blot. Protein lysates from cells or tumor tissues were prepared using lysis buffer [50 mM tris-HCl (pH 7.5), 150 mM NaCl, 1% NP-40, 0.5% Na-deoxycholate] containing Protease and Phosphatase Inhibitor Cocktail (Bimake). Protein concentration was measured by DC Protein Assay (Bio-Rad). 20-80 µg of protein lysates were separated by sodium dodecyl sulfate polycrylamide gel electrophoresis (SDS-PAGE) and transferred to equilibrated nitrocellulose membrane (Bio-Rad Laboratories). After blocking with 5% non-fat milk in 1 × TBST, membranes were probed with primary antibodies overnight at 4°C, followed by secondary antibodies conjugated with horseradish peroxidase (HRP) for 2 hours at room temperature. Antibody-antigen complexes were detected with Enhanced Chemiluminescence (GE Healthcare Life Sciences) and

ChemDoc Imaging System (Bio-Rad). Signals were quantified by Image J software and defined as the ratio of target protein relative to GAPDH. The antibodies used for western blot are listed in **supplementary table 3**.

ScRNA-seq. ScRNA-seq was performed on tumor cell lines or single cells isolated from tumor tissues of Hepa1-6 PD-L1S and PD-L1R-tumor-bearing mice as well as needle biopsies from HCC patients in the pembrolizumab trial (NCT03419481). In brief, Hepa1-6 PD-L1S and PD-L1R-tumor-bearing mice were treated with 3-dose anti-PD-L1 and tumors were collected at day 18 post tumor-inoculation. Pre-treatment and on-treatment tumor biopsies from HCC or chopped mouse tumor tissues were enzymatically digested in 5 ml buffer from Tumor Dissociation Kit (Miltenyi Biotec) at 37 °C for 20 min with 300 rpm on Eppendorf ThermoMixer C. Cells were then collected and red blood cells were removed by ACK Lysis Buffer (ThermoFisher Scientific). Cells were passed through a 100-μm cell strainer (BD Biosciences) followed by evaluation of cell viability via trypan blue staining. Single-cell libraries were prepared by Chromium Single Cell 3' Library and Gel Bead Kit v2 or v3 (10× Genomics). Briefly, cell suspensions were loaded onto a Chromium Single Cell Chip along with the reverse transcription (RT) mix and single cell 3' gel beads, aiming for 5,000 cells per channel. After RT, cDNA generated within individual Bead-In-Emulsion (GEM) was tagged with a common 10× barcode and a unique molecular identifier (UMI). Thirteen-fifteen cycles were used for cDNA amplification, and purification was conducted using SPRI select beads (Beckman Coulter), as per the manufacturer's recommended parameters. Following the cDNA-amplification reaction, quality control and quantification was performed on the Agilent 2100 bioanalyzer using the High Sensitivity D5000 chip (Agilent Technologies). Illumina sequencing libraries were constructed by fragmentation, end repair, A-tailing double-

Supplemental material

BMJ Publishing Group Limited (BMJ) disclaims all liability and responsibility arising from any reliance placed on this supplemental material which has been supplied by the author(s)

Gut

sided size selection, adaptor ligation and sample-index PCR. Quality control and quantification of final libraries were performed on the Agilent 2100 Bioanalyzer using the High Sensitivity D1000 chip (Agilent Technologies) and KAPA Library Quantification Kit (KAPA Biosystems). Libraries were then sequenced on NovaSeq 6000, HiSeq 4000 or NextSeq 500 (Illumina) with 150-bp paired-end reads until sufficient saturation was reached.

ScRNA-seq analysis. Sequencing raw data were aligned to the human reference genome (GRCh38) or mouse reference genome (mm10) for UMI count quantification using Cell Ranger (10× Genomics, v4.0.0). All samples had good sequencing yield, with raw reads ranging from 80–264 million per sample and > 95% Q30 bases in barcode. Background noise in human scRNA-seq data was removed using CellBender 0.2.0 with default parameters if appropriate[10]. For quality control, we removed cells with low quality reads according to the following criteria: 1) Number of expressed genes < 200; 2) Percentage of mitochondrial genes ≥ 20%. 3) Number of UMIs < 500.

For mouse scRNA-seq data, dimension reduction was performed by UMAP following workflow in Cell Ranger. To cluster single cells based on gene expression profiles, a graph-based clustering algorithm implemented in Cell Ranger pipeline (v4.0.0). Major cell types were annotated based on distributions of canonical marker genes. To confirm the identity of cells within each cluster, we examined the expression levels of canonical marker for liver tumor cells[11], B cells[12], endothelial cell[1 13 14], erythroid cell[15], fibroblast[1], macrophage/DC[12], MDSC-like cell[16], T/NK cell[12] with sufficient references. We identified differentially expressed genes (DEGs) generated by Cell Ranger according to the following criteria: 1) P-value < 0.05; 2) Normalized expression > 0.1; 3) Log_2fold-change > 0.5. KEGG pathway enrichment analysis of DEGs between PD-L1S and PD-

L1R tumor cells was performed by Enrichr Web Platform (https://maayanlab.cloud/Enrichr/). Gene set enrichment analysis (GSEA) was performed for ranked list of DEGs against PPAR hallmark gene sets from KEGG database.

For scRNA-seq data of Hepa1-6 PD-L1S and –PD-L1R tumor cell lines, we used Seurat v4 (v4.1.2) to perform data filtering (both gene and cell), normalization and principal component analysis. GSEA was performed for ranked list of all genes against PPAR hallmark gene sets from KEGG database.

For human scRNA-seq analysis, Seurat v3 (v3.2.2) was applied for the identification of variable features (FindVariableFeatures), data normalization (NormalizeData), scaling (ScaleData), and principal component analysis (RunPCA), dimension reducntion (RunUMAP) and unsupervised graph-based clustering (FindNeighbors & FindClusters). Top marker genes were identified for each cluster (FindAllMarkers).

Online patient dataset analysis. mRNA levels and survival data of liver hepatocellular carcinoma (LIHC) from The Cancer Genome Atlas (TCGA) was obtained from the University of California, Santa Cruz (UCSC; http://xena.ucsc.edu/). LIHC samples were stratified into high (15%) and low (85%) groups according to mRNA level of *PPARA*, *PPARG* or *VEGF-A*[17]. To evaluate the associations of PPARα or PPARγ and CD8^{+} T cell dysfunction, GSEA (https://www.gsea-msigdb.org/gsea) was performed on normalized gene list with 1000 permutations. Enrichment scores were computed with a positive or negative value to compare the enrichment level of dysfunctional CD8^{+} T cell signature between high versus low group. Gene sets with nominal $P <$

8

Supplemental material

BMJ Publishing Group Limited (BMJ) disclaims all liability and responsibility arising from any reliance placed on this supplemental material which has been supplied by the author(s)

Gut

0.05 and FDR < 0.25 were considered significant. Patients in high or low group were then compared for their overall survival and plotted in standard Kaplan-Meier curves. To explore the potential roles of PPARα, PPARγ or VEGF-A on tumor immune evasion, TIDE, T cell exclusion and MDSC signatures were calculated by TIDE algorithm (http://tide.dfci.harvard.edu/), according to the developer's instructions. The cutoff value of 0 in TIDE score was used to predict ICB response of each tumor sample. To study the correlation between PPARγ and survival in ICB-treated patients, patients were classified into high and low groups based on the optimal cutoff threshold for each individual ICB cohort via z-score in Cox proportional hazard model. Overall and progression-free survival analysis was then visualized by Kaplan-Meier plots. To investigate the correlation between PPARγ and VEGF-A, their gene expression levels in tumor cells of our in-house and a public[1] dataset of human liver cancer scRNA-seq were evaluated.

ChIP-qPCR assay. Chromatin immunoprecipitation (ChIP) was conducted as described previously[19]. Briefly, cells were directly cross-linked by 1% formaldehyde and the reaction was stopped by glycine at room temperature. Fixed cells were lysed on ice for 5 min with 1% SDS lysis buffer containing proteinase inhibitor (Thermo Fisher Scientific). The lysates were fragmented to 200-300 base pairs (bp) by Bioruptor (Diagenode). The ChIP-graded anti-PPARγ antibody (Cell Signaling Technology) or normal rabbit IgG (Cell Signaling Technology) were conjugated with magnetic beads (Magna ChIP Protein A+G Magnetic Beads, Life Technologies) by rotation in cold room (4°C) for 1 hour. The cell lysate were incubated with magnetic beads-conjugated antibodies and rotated in cold room for 12 to 16 hours. After washing, elution and reverse-crosslink, the immunoprecipitated DNA were purified by QIAquick PCR Purification Kit (QIAGEN). The ChIP-enriched chromatin was further analyzed by Real-Time PCR with Power

SYBR Green Master Mix (Applied Biosystems) and normalized to the input DNA. The primer sequences for ChIP-qPCR are listed in **supplementary table 2**.

Flow cytometry. Primary single cells were isolated from fresh tumor tissues by Tumor Dissociation Kit (Miltenyi Biotec) and gentleMACS dissociators (Miltenyi Biotec) following manufacturer's instructions. Cells were collected and washed, then incubated with 2.4G2 mAb for 15 min at 4°C to block Fc gamma receptors. For cell-surface staining, cells were directly stained with fluorochrome-conjugated antibodies at optimum concentration for 20 min at room temperature. For intracellular staining, cells were permeabilized by CytoFix/CytoPerm buffer (BD Bioscience) for 20 min at 4°C. After washing by Perm Wash Buffer (BD Bioscience), the cells were incubated in indicated conjugated antibodies for 1 hour at 4°C. For cell apoptosis analysis, cells were initially stained with anti-CD45 antibodies for 20 min, and then washed and stained by Annexin V-FITC Apoptosis Detection Kit (Abcam) according to the manufacturer's instructions. Flow cytometry data were acquired by FACSAria Fusion (BD Biosciences) and analyzed by FlowJo software (Tree Star). The antibodies used for flow cytometry are listed in **supplementary table 3**.

Ev vivo **T-cell suppressive assay.** To study the immunosuppressive activity of tumoral PMN-MDSCs, $CD45^+CD11b^+Gr-1^+Ly6G^+Ly6C^{-/low}$ PMN-MDSCs were sorted from tumors of Hepa1-6 PD-L1R-shNC or -shPPARγ-tumor bearing mice by FACS. $CD8^+$ T cells were purified from naïve mouse spleen by anti-mouse CD8 microbeads and co-cultured with sorted PMN-MDSCs (1:1) in the presence of CD3/CD28 dynabeads (Invitrogen) and mouse recombinant IL-2 (R&D) for 3 days. T cells with or without dynabead stimulation was used as positive or negative control,

respectively. Surface staining for CD3/CD4/CD8 T cell markers and intracellular staining for Ki-67/IFN-γ/TNF-α in T cells were acquired by flow cytometry using FACSymphony™ A5.2 Cell Analyzer (BD Biosciences). The proliferation and function of T cells were determined and calculated by FlowJo software (Tree Star).

Enzyme-linked immunosorbent assay (ELISA). The concentration of VEGF-A in cell or tumor tissue lysates was detected by Mouse VEGF Duoset ELISA Kit (R&D) following the manufacturer's instructions. For tumor cell lysates, 8×10^6 cells were collected and incubated in [50 mM tris-HCl (pH 7.5), 150 mM NaCl, 1% NP-40, 0.5% Na-deoxycholate] supplemented with Protease and Phosphatase Inhibitor Cocktail (Bimake) on ice for 30 min. The concentration of protein supernatants was determined by DC Protein Assay Kit (Bio-Rad), followed by normalization of protein loading for each group. For tumor tissue lysates, 80 mg tumor tissues were homogenized and lysed by lysis buffer containing protease and phosphatase inhibitors on ice, followed by centrifugation for collecting supernatants.

***Ex vivo* myeloid cell and T cell functional assays.** Conditional media (CM) of Hepa1-6 PD-L1R-shNC and -shPPARγ cells were harvested at 48 hours after *in vitro* culture. For *ex vivo* myeloid cell assay, naïve bone marrow cells or blood-derived CD11b$^+$ cells isolated by CD11b MicroBeads (Miltenyi Biotec) were cultured in CM containing GM-CSF (20 ng/ml) supplied with or without recombinant VEGF-A protein (100 ng/ml, R&D) for 4 days. The proportion, phenotype and immunosuppressive function of PMN-MDSCs, macrophages and DCs were analysed by flow cytometry using antibodies against mouse CD45, CD11b, Gr-1, F4/80, CD11c, Ly-6G, Ly-6C, Arg-1, CD80, CD86, MHC I, MHC II, iNOS and CD206. For *ex vivo* T cell assay, CD8$^+$ T cells were purified from the spleen of subcutaneous Hepa1-6 (1×10^7)-tumor bearing mice via CD8a

MicroBeads (Miltenyi Biotec) and then incubated with conditional supernatant supplied with or without 100 ng/ml recombinant mouse VEGF-A protein for 4 days. The expression levels of exhaustion and effector markers on CD8$^+$ T cells were accessed by flow cytometry using antibodies against mouse CD3, CD8, PD-1, TIM-3, IFN-γ and TNF-α.

H&E and immunofluorescence staining. Tumor biopsies from patients or mouse liver tumor tissues were collected and fixed in 4% paraformaldehyde (Sigma-Aldrich) for 24 hours, washed in 70% ethanol and embedded in paraffin. Five-millimeter sections from paraffin embedded tumor biopsies were deparaffinized, rehydrated, and rinsed in distilled water. The sections were then stained with H&E. Immunofluorescence staining was performed manually using the Opal 7-Color IHC Kits (PerkinElmer) according to manufacturer's protocol against the immune markers at specific dilutions: cleaved caspase-3 (1:200), CK8/18 (1:50), CD11b (1:500), CD15 (1:500), CD8a (1:200), PPARγ (1:100) and Ly-6G (1:200). Opal 520 (1:500), Opal 650 (1:200) and Opal 570 (1:200) were used and the slides were counterstained with DAPI and mounted with VECTASHIELD Antifade Mounting Medium. Images were captured by Axio Observed Z1 and Axioscan 7 Automatic Slide Scanner (Zeiss, Germany). The antibodies used for immunofluorescence staining are listed in **supplementary table 3**.

Toxicity evaluation. To determine potential toxicity-associated tissue damage caused by T0070907, the liver, spleen, kidney and heart were weighted and fixed in 10% formalin for subsequent paraffin embedding. Five paraffin sections per each organ were stained with H&E and examined by a pathologist who was blinded to the treatment status of the samples. Further, mouse serum concentrations of alanine aminotransferase (ALT) and aspartate aminotransferase (AST)

12

were measured using Alanine Transaminase Activity Assay Kit (ab105134; Abcam) and Aspartate Aminotransferase Activity Assay Kit (ab105135; Abcam), respectively, according to the manufacturer's protocol.

Statistical analysis. Data were analyzed using GraphPad Prism 8 and are presented as mean ± SD. Statistical comparison between groups was evaluated by two-tailed and unpaired Student's t test. Paired Student's t test was used to compare pre-treatment and on-treatment samples. Correlation analysis was performed using single-tailed Pearson correlation. Kaplan-Meier survival analysis was performed by log-rank (Mantel-Cox) test. The relationship between two categorical variables were computed by Chi-square test. *P* value smaller than 0.05 was considered statistically significant.

Supplemental material

BMJ Publishing Group Limited (BMJ) disclaims all liability and responsibility arising from any reliance placed on this supplemental material which has been supplied by the author(s)

Gut

Supplementary References

1 Ma L, Hernandez MO, Zhao Y, *et al*. Tumor Cell Biodiversity Drives Microenvironmental Reprogramming in Liver Cancer. Cancer cell 2019;36:418-30 e6.

2 Zhou J, Liu M, Sun H, *et al*. Hepatoma-intrinsic CCRK inhibition diminishes myeloid-derived suppressor cell immunosuppression and enhances immune-checkpoint blockade efficacy. Gut 2018;67:931-44.

3 Kwong TT, Wong CH, Zhou JY, *et al*. Chemotherapy-induced recruitment of myeloid-derived suppressor cells abrogates efficacy of immune checkpoint blockade. JHEP reports : innovation in hepatology 2021;3:100224.

4 Zeng X, Zhou J, Xiong Z, *et al*. Cell cycle-related kinase reprograms the liver immune microenvironment to promote cancer metastasis. Cellular & molecular immunology 2021;18:1005-15.

5 Wen L, Xin B, Wu P, *et al*. An Efficient Combination Immunotherapy for Primary Liver Cancer by Harmonized Activation of Innate and Adaptive Immunity in Mice. Hepatology 2019;69:2518-32.

6 Zhang Q, Ma C, Duan Y, *et al*. Gut Microbiome Directs Hepatocytes to Recruit MDSCs and Promote Cholangiocarcinoma. Cancer Discov 2021;11:1248-67.

7 Bray NL, Pimentel H, Melsted P, *et al*. Near-optimal probabilistic RNA-seq quantification. Nature biotechnology 2016;34:525-7.

8 Love MI, Huber W, Anders S. Moderated estimation of fold change and dispersion for RNA-seq data with DESeq2. Genome biology 2014;15:550.

9 Talevich E, Shain AH, Botton T, *et al*. CNVkit: Genome-Wide Copy Number Detection and Visualization from Targeted DNA Sequencing. PLoS computational biology 2016;12:e1004873.

10 Fleming SJ, Marioni JC, Babadi M. CellBender remove-background: a deep generative model for unsupervised removal of background noise from scRNA-seq datasets. bioRxiv 2019:791699.

11 Zheng H, Pomyen Y, Hernandez MO, *et al*. Single-cell analysis reveals cancer stem cell heterogeneity in hepatocellular carcinoma. Hepatology 2018;68:127-40.

12 Zhang Q, He Y, Luo N, *et al*. Landscape and Dynamics of Single Immune Cells in Hepatocellular Carcinoma. Cell 2019;179:829-45 e20.

13 Goveia J, Rohlenova K, Taverna F, *et al*. An Integrated Gene Expression Landscape Profiling Approach to Identify Lung Tumor Endothelial Cell Heterogeneity and Angiogenic Candidates. Cancer cell 2020;37:421.

14 Su SC, Mendoza EA, Kwak HI, *et al*. Molecular profile of endothelial invasion of three-dimensional collagen matrices: insights into angiogenic sprout induction in wound healing. American journal of physiology Cell physiology 2008;295:C1215-29.

15 Lambrechts D, Wauters E, Boeckx B, *et al*. Phenotype molding of stromal cells in the lung tumor microenvironment. Nature medicine 2018;24:1277-89.

16 Alshetaiwi H, Pervolarakis N, McIntyre LL, *et al*. Defining the emergence of myeloid-derived suppressor cells in breast cancer using single-cell transcriptomics. Science immunology 2020;5.

17 Cerezo-Wallis D, Contreras-Alcalde M, Troule K, *et al*. Midkine rewires the melanoma microenvironment toward a tolerogenic and immune-resistant state. Nature medicine 2020;26:1865-77.

18   Jiang P, Gu S, Pan D, *et al*. Signatures of T cell dysfunction and exclusion predict cancer immunotherapy response. Nature medicine 2018;24:1550-8.

19   Yang W, Feng Y, Zhou J, *et al*. A selective HDAC8 inhibitor potentiates antitumor immunity and efficacy of immune checkpoint blockade in hepatocellular carcinoma. Science translational medicine 2021;13.

Supplementary Tables

Supplementary Table 1. KEGG pathway analysis of DEGs between PD-L1S and PD-L1R tumor cells.

Term	Overlap	P-value	Adjusted P-value	Odds Ratio	Combined Score	Genes
Top 5 enriched pathways in PD-L1R tumor cells						
PPAR signaling pathway	19/74	3.72×10^{-9}	1.09×10^{-6}	6.50	126.23	GK; APOA2; APOA1; LPL; APOC3; CYP27A1; FABP1; RXRA; FABP4; ACADL; ACOX2; FABP5; ACSBG1; PLIN2; PPARG; ACADM; HMGCS2; ANGPTL4; PPARA
Cholesterol metabolism	15/50	1.64×10^{-8}	2.40×10^{-6}	8.05	144.24	APOA2; APOA1; LCAT; LPL; APOC3; CYP27A1; NPC1; VAPA; APOH; APOC2; ANGPTL8; APOC1; ANGPTL4; LDLRAP1; APOB
Complement and coagulation cascades	17/85	1.18×10^{-6}	1.16×10^{-4}	4.69	64.06	FGB; FGA; SERPIND1; SERPINC1; SERPINE1; FGG; SERPINF2; CFI; F11; F2; KNG1; F5; C4B; C3; VTN; PROC; SERPING1
Protein processing in endoplasmic reticulum	22/171	6.43×10^{-5}	4.71×10^{3}	2.77	26.78	PPP1R15A; TRAM1; HSPA5; DERL3; HSPA4L; SEL1L; RRBP1; UBE2G2; PDIA4; HERPUD1; DNAJC3; SEC61A1; LMAN1; DDIT3; DNAJC5; FBXO6; STT3B; P4HB; SEC24D; SIL1; ATF4; TXNDC5
Valine, leucine and isoleucine degradation	10/48	1.31×10^{-4}	6.52×10^{3}	4.91	43.95	BCKDHA;HMGCL;ACAA2;ECHS1; AUH; AGXT2;AOX1;ACADM; HMGCS2;ACADSB
Top 5 enriched pathways in PD-L1S tumor cells						
Cell cycle	57/124	1.95×10^{-18}	6.04×10^{-16}	5.50	224.45	YWHAE; MCM7; CCNH; BUB1B; CDC14A; CDC23; CCND1; PTTG1; YWHAQ; CDC26; MYC; CHEK1; SKP2; YWHAH; SMC1A; CDC25B; CCNA2; DBF4; RBL1; TFDP1; CCNE2; MCM3; ANAPC4; MCM4; ANAPC5; MCM5; MCM6; MAD1L1; MCM2; ANAPC13; HDAC2; PCNA; HDAC1; PKMYT1; ANAPC10; ANAPC11; ORC4; FZR1; CDC45; ORC3; ORC2; E2F3; BUB3; E2F4; BUB1; CDKN2B; SMAD3; TGFB1; CDKN2C; CDKN2A; PLK1; CDC6; STAG1; CDK2; CDK1; ATM; MAD2L1
DNA replication	26/36	1.66×10^{-15}	2.57×10^{-13}	16.68	567.70	PRIM2; RNASEH2C; FEN1; RNASEH2B; PCNA; MCM7; PRIM1; POLD1; POLD2; RFC5; RFC3; LIG1; RFC1; RFC2; RPA1; RPA2; POLE4; POLA1; POLA2; RPA3; MCM3; MCM4; MCM5; MCM6; SSBP1; MCM2

Spliceosome	53/150	1.24×10^{-11}	1.28×10^{-9}	3.52	88.47	EIF4A3; PRPF19; PQBP1; EFTUD2; MAGOH; SNRPD3; TXNL4A; AQR; NCBP1; NCBP2; BUD31; CRNKL1; PRPF4; RBMXL1; DDX39B; PRPF3; SNRPG; SRSF2; SNRNP27; SRSF3; PPIH; SNRPF; SNRPC; SRSF6; SRSF7; SRSF9; SF3B4; SF3B5; RBM8A; SF3B6; SRSF1; PRPF8; U2AF2; TRA2A; HSPA8; PRPF38B; PPIL1;P RPF38A; SF3A2; FUS; ALYREF; CDC5L; LSM5; LSM3; LSM2; HNRNPM; LSM7; SNRNP40; LSM6; ACIN1; PRPF31; HNRNPC; RBMX
Mismatch repair	16/23	1.23×10^{-9}	9.56×10^{-8}	14.61	299.77	RFC5; RFC3; PCNA; LIG1; RFC1; RFC2; RPA1; RPA2; MSH6; MSH2; EXO1; MSH3; POLD1; RPA3; POLD2; SSBP1
RNA transport	53/186	6.96×10^{-8}	4.31×10^{-6}	2.56	42.26	POP5; NUP107; NXT1; NUP188; POP1; POP4; RPP30; EIF4A3; CASC3; XPO1; SUMO1; MAGOH; SUMO2; XPO5; NDC1; PRMT5; NCBP1; NUP133; EIF1AX; NCBP2; TRNT1; RPP25L; NUP93; DDX39B; GEMIN5; GEMIN6; GEMIN8; KPNB1; NUP205; POM121; RBM8A; AAAS; NUP160; NUP85; TGS1; NUP43; RPP14; PAIP1; EIF2B4; NUP155; FUS; ALYREF; UPF3B; EIF2S1; TACC3; ACIN1; NUP35; RNPS1; TARDBP; EIF4G3; EIF3A; RAN; NUP37

17

Supplementary Table 2. Primers used in this study.

Species	Gene	Primer	Sequence	Application
Mouse	*Areg*	Forward	GCAGATACATCGAGAACCTGGAG	RT-qPCR
		Reverse	CCTTGTCATCCTCGCTGTGAGT	
	Btc	Forward	TTCGTGGTGGACGAGCAAACTC	RT-qPCR
		Reverse	CCATGACCACTATCAAGCAGACC	
	Cmtm8	Forward	CTTCGCTTACGACCGAGAGTTC	RT-qPCR
		Reverse	CCAGCCAAAAGCAGGGACTCTA	
	Gapdh	Forward	CATCACTGCCACCCAGAAGACTG	RT-qPCR
		Reverse	ATGCCAGTGAGCTTCCCGTTCAG	
	Gdf15	Forward	AGCCGAGAGGACTCGAACTCAG	RT-qPCR
		Reverse	GGTTGACGCGGAGTAGCAGCT	
	Il33	Forward	CTACTGCATGAGACTCCGTTCTG	RT-qPCR
		Reverse	AGAATCCCGTGGATAGGCAGAG	
	Nrg4	Forward	GAGACAAACAATACCAGAAC	RT-qPCR
		Reverse	GGACTGCCATAGAAATGA	
	Osgin1	Forward	AGACTCTGTGCTCTCCTGGAAG	RT-qPCR
		Reverse	GCCTTGGCTCAAGGTCACCATG	
	Pparg	Forward	GGAATCAGCTCTGTGGACCT	RT-qPCR
		Reverse	CCTGTTGTAGAGCTGGGTCT	
	Qrfp	Forward	CCTATGTTTCTCAGAACGAGTGTG	RT-qPCR
		Reverse	TAGGAGACTCGGCAGCCTTTGA	
	Sema4g	Forward	TTCATGGAGCGTGAGGAAGGCT	RT-qPCR
		Reverse	TGGCAGATGAGACGAGCCTTCA	
	Stc1	Forward	AGGAGGACTGCTACAGCAAGCT	RT-qPCR
		Reverse	TCCAGAAGGCTTCGGACAAGTC	
	Tgfa	Forward	CAGGCTCTGGAGAACAGCACAT	RT-qPCR
		Reverse	GACACATGCTGGCTTCTCTTCC	
	Thpo	Forward	TGCTGTGGACTTTAGCCTGGGA	RT-qPCR
		Reverse	ATGAGAGGCAGGAGGGTTCCAA	
	Vegfa	Forward	CGGTTTGAGGAGGTTGGTTC	RT-qPCR
		Reverse	CCCAAAAGCAGGTCAGTCAC	
	Vegfa	Forward	GTCCTCCCTCACGCAGACTCG	ChIP-qPCR
		Reverse	GAATCAACTCTCACCCCCTTT	

Supplementary Table 3. Antibodies used in this study.

Western blot						
Species	Fluorophore	Antibody	Clone	Vendor	Catalog number	Recommended concentration
anti-mouse/human		GAPDH		Millipore	MAB374	1:1000
anti-mouse/human		PPARα		Santa Cruz Biotechnology	sc-398394	1:500
anti-mouse/human		PPARγ		Cell signaling Technology	2443	1:1000
ChIP						
Species	Fluorophore	Antibody	Clone	Vendor	Catalog number	Recommended concentration
		Normal Rabbit IgG		Cell signaling Technology	2729	10 μg/ChIP
anti-mouse/human		PPARγ		Santa Cruz Biotechnology	sc-7373 X	10 μg/ChIP
Immunofluorescence						
Species	Fluorophore	Antibody	Clone	Vendor	Catalog number	Recommended concentration
anti-mouse/human		CD11b		Abcam	ab133357	1:500
anti-human		CD8α		Cell signaling Technology	70306	1:200
anti-human		CD15		Abcam	Ab665	1:200
anti-mouse/human		Cleaved caspase-3		Cell signaling Technology	9661S	1:200
anti-mouse/human		Cytokeratin 8		ABclonal	A1024	1:50
anti-mouse/human		Cytokeratin 18		ABclonal	A1022	1:50
anti-mouse/human		PPARγ		Cell signaling Technology	2443	1:100
Flow cytometry						
Species	Fluorophore	Antibody	Clone	Vendor	Catalog number	Recommended concentration
anti-mouse	APC-eFlour 780	Arginase 1	A1exF5	Thermo Fisher Scientific	25-3697-82	2.5 μl/10^6 cells
anti-mouse	PerCP-eFluor 710	Arginase 1	A1exF5	Thermo Fisher Scientific	46-3697-82	0.8 μl/10^6 cells
	FITC	Carboxy-H2DFFDA		Thermo Fisher Scientific	C13293	10 μM
anti-mouse	Alexa Fluor 488	CD107a	eBio1D4B (1D4B)	Thermo Fisher Scientific	53-1071-80	0.3 μl/10^6 cells
anti-mouse	Brilliant Violet 711	CD11b	M1/70	BD	563168	0.3 μl/10^6 cells
anti-mouse	PE	CD11b	M1/70	Thermo Fisher Scientific	12-0112-82	0.625 μl/10^6 cells
anti-mouse	APC	CD11c	N418	Thermo Fisher Scientific	17-0114-82	1.25 μl/10^6 cells

19

anti-mouse	BUV563	CD11c	N418	BD	749040	0.3 µl/10^6 cells
anti-mouse	APC	CD206	C068C2	BioLegend	141708	0.6 µl/10^6 cells
anti-mouse	APC-eFlour 780	CD25	PC61.5	Thermo Fisher Scientific	47-0251-82	2.5 µl/10^6 cells
anti-mouse	PE-Cy5	CD3	17A2	BioLegend	100218	1 µl/10^6 cells
anti-mouse	eFluor 450	CD3	17A2	Thermo Fisher Scientific	48-0032-82	2.5 µl/10^6 cells
anti-mouse	Brilliant Violet 605	CD3	145-2C11	BioLegend	100351	2.5 µl/10^6 cells
anti-mouse	Brilliant Violet 421	CD4	RM4-5	BioLegend	100563	1.25 µl/10^6 cells
anti-mouse	BB750	CD4	RM4-5	BD	624391	0.3 µl/10^6 cells
anti-mouse	PE-Cy5	CD44	IM7	Thermo Fisher Scientific	15-0441-82	0.3 µl/10^6 cells
anti-mouse	BUV805	CD45	30-F11	BD	748370	0.3 µl/10^6 cells
anti-mouse	Brilliant Violet 711	CD45	30-F11	BioLegend	103147	1.25 µl/10^6 cells
anti-mouse	FITC	CD45	30F11	Thermo Fisher Scientific	11-0451-82	1 µl/10^6 cells
anti-mouse	Brilliant Violet 650	CD80	16-10A1	BioLegend	104732	0.8 µl/10^6 cells
anti-mouse	PE-Cy7	CD86	GL1	BD	560582	0.3 µl/10^6 cells
anti-mouse	APC-eFluor 780	CD8α	53-6.7	Thermo Fisher Scientific	47-0081-82	2.5 µl/10^6 cells
anti-mouse	BB790	CD8α	53-6.7	BD	624296	0.3 µl/10^6 cells
anti-mouse	FITC	CD8α	53-6.7	BioLegend	100705	2 µl/10^6 cells
anti-mouse	PE	CTLA-4	UC10-4B9	Thermo Fisher Scientific	12-1522-82	1.25 µl/10^6 cells
anti-mouse	APC-eFluor 780	F4/80	BM8	Thermo Fisher Scientific	47-4801-82	2.5 µl/10^6 cells
anti-mouse	BUV395	F4/80	T45-2342	BD	565614	0.3 µl/10^6 cells
	440UV	Fixable Viability Stain		BD	566332	0.2 µl/10^6 cells
anti-mouse	PE	FOXP3	FJK-16s	Thermo Fisher Scientific	12-5773-82	5 µl/10^6 cells
anti-mouse	BUV737	Gr-1	RB6-BC5	BD	741712	0.4 µl/10^6 cells
anti-mouse	PE-Cy5	Gr-1	RB6-8C5	BioLegend	108410	1.25 µl/10^6 cells
anti-mouse	APC/Fire750	Granzyme B	QA16A02	BioLegend	372210	1.25 µl/10^6 cells
anti-mouse	PE-Cy7	Granzyme B	NGZB	Thermo Fisher Scientific	25-8898-82	0.625 µl/10^6 cells
anti-mouse	Brilliant Violet 750	IFN-γ	XMG1.2	BD	566366	0.4 µl/10^6 cells
anti-mouse	PE	IFN-γ	XMG1.2	Thermo Fisher Scientific	12-7311-82	1.25 µl/10^6 cells
anti-mouse	FITC	IL-2	JES6-5H4	Thermo Fisher Scientific	11-7021-41	5 µl/10^6 cells
anti-mouse	Alexa Fluor 700	iNOS	CXNFT	Thermo Fisher Scientific	56-5920-82	0.3 µl/10^6 cells

20

Supplemental material

BMJ Publishing Group Limited (BMJ) disclaims all liability and responsibility arising from any reliance placed on this supplemental material which has been supplied by the author(s)

Gut

anti-mouse	PE	Ki-67	SolA15	Thermo Fisher Scientific	12-5698-82	0.3 μl/10^6 cells
anti-mouse	FITC	LAG-3	C9B7W	Thermo Fisher Scientific	11-2231-82	2 μl/10^6 cells
anti-mouse	Brilliant Violet 605	Ly-6C	AL-21	BD	563011	0.5 μl/10^6 cells
anti-mouse	eFluor 450	Ly-6C	HK1.4	Thermo Fisher Scientific	48-5932-82	1.25 μl/10^6 cells
anti-mouse	Brilliant Violet 510	Ly-6G	1A8	BD	740157	0.5 μl/10^6 cells
anti-mouse	Brilliant Violet 605	Ly-6G	1A8	BioLegend	127639	1.25 μl/10^6 cells
anti-mouse	FITC	MHC class I	34-1-2S	Thermo Fisher Scientific	11-5998-82	0.8 μl/10^6 cells
anti-mouse	BUV496	MHC class II	M5/114	BD	750281	0.3 μl/10^6 cells
anti-mouse	APC	PD-1	J43	Thermo Fisher Scientific	17-9985-82	2.5 μl/10^6 cells
anti-mouse	BUV615	PD-1	RMP1-30	BD	752354	0.4 μl/10^6 cells
anti-mouse	Brilliant Violet 605	PD-1	29F.1A12	BioLegend	135220	0.625 μl/10^6 cells
anti-mouse	PerCP-eFluor 710	PD-L1	MIH5	Thermo Fisher Scientific	46-5982-82	0.625 μl/10^6 cells
anti-mouse	Alexa-Fluor 647	S100A9	2B10	BD Pharmingen	2B10	0.625 μl/10^6 cells
anti-mouse	PE-Cy7	T-bet	4B10	BioLegend	644823	1.25 μl/10^6 cells
anti-mouse	BB700	TIM-3	5D12	BD	747619	0.5 μl/10^6 cells
anti-mouse	PerCP-Cy5.5	TIM-3	B8.2C12	BioLegend	134012	1.25 μl/10^6 cells
anti-mouse	APC	TNF-α	MP6-XT22	Thermo Fisher Scientific	17-7321-82	1.25 μl/10^6 cells
anti-mouse	Brilliant Violet 421	TNF-α	MP6-XT22	BD	563387	0.4 μl/10^6 cells
anti-mouse	PE	VEGFR2	Avas12	BioLegend	136403	5 μl/10^6 cells